Acta Geologica Sinica (English Edition), 2019, 93(2): 344–361

Petrology and Geochemistry of the Dangqiong Ophiolite, Western Yarlung-Zangbo Suture Zone, Tibet, China

XU Xiangzhen[1, *], YANG Jingsui[1], XIONG Fahui[1] and GUO Guolin[2]

[1] *CARMA (Center for Advanced Research on Mantle), Key Laboratory of Deep-Earth Dynamics of Ministry of Natural Resources, Institute of Geology, Chinese Academy of Geological Sciences, Beijing 100037, China*
[2] *State Key Laboratory Breeding Base of Nuclear Resources and Environment, East China Institute of Technology, Nanchang 330013, China*

Abstract: The Dangqiong ophiolite, the largest in the western segment of the Yarlung-Zangbo Suture Zone (YZSZ) ophiolite belt in southern Tibet, consists of discontinuous mantle peridotite and intrusive mafic rocks. The former is composed dominantly of harzburgite, with minor dunite, locally lherzolite and some dunite containing lenses and veins of chromitite. The latter, mafic dykes (gabbro and diabase dykes), occur mainly in the southern part. This study carried out geochemical analysis on both rocks. The results show that the mantle peridotite has Fo values in olivine from 89.92 to 91.63 and is characterized by low aluminum contents (1.5–4.66 wt%) and high $Mg^{\#}$ values (91.06–94.53) of clinopyroxene. Most spinels in the Dangqiong peridotites have typical $Mg^{\#}$ values ranging from 61.07 to 72.52, with corresponding $Cr^{\#}$ values ranging from 17.67 to 31.66, and have TiO_2 contents from 0 to 0.09%, indicating only a low degree of partial melting (10–15%). The olivine-spinel equilibrium and spinel chemistry of the Dangqiong peridotites suggest that they originated deeper mantle (>20 kbar). The gabbro dykes show N-MORB-type patterns of REE and trace elements. The presence of amphibole in the Dangqiong gabbro suggests the late-stage alteration of subduction-derived fluids. All the lherzolites and harzburgites in Dangqiong have similar distribution patterns of REE and trace elements, the mineral chemistry in the harzburgites and lherzolites indicates compositions similar to those of abyssal and forearc peridotites, suggesting that the ophiolite in Dangqiong formed in a MOR environment and then was modified by late-stage melts and fluids in a suprasubduction zone (SSZ) setting. This formation process is consistent with that of the Luobusa ophiolite in the eastern Yarlung-Zangbo Suture Zone and Purang ophiolite in the western Yarlung-Zangbo Suture Zone.

Key words: gabbro, mantle peridotite, Dangqiong ophiolite, Yarlung-Zangbo Suture Zone, Tibet

Citation: Xu et al., 2019. Petrology and Geochemistry of the Dangqiong Ophiolite, Western Yarlung-Zangbo Suture Zone, Tibet, China. *Acta Geologica Sinica* (English Edition), 93(2): 344–361. DOI: 10.1111/1755-6724.13806

1 Introduction

Ophiolites represent the remnants of ancient oceanic lithospheric fragments in a continental orogenic belt, and contain important information about the magmatic evolution, metamorphism and tectonic processes of the oceanic lithosphere and are thus important units for understanding the evolution and closure of ancient oceanic basins. The ophiolite is usually divided into four units: metamorphic peridotite, a deep plutonic complex, a sheeted dyke group and extrusive rock (Coleman, 1977; Zhang et al., 2000). Dyke intrusions, including those of pyroxenite, gabbro and diabase, are common in metamorphic peridotite and considered to be the magmatic rocks produced by partial melting of the mantle. The Yarlung-Zangbo Suture Zone (YZSZ), which is located in the southern region of Tibet, represents the boundary between the Eurasian plate and the Indian plate. Late Jurassic to Early Cretaceous ophiolite blocks are widely distributed along the YZSZ and are the remains of the Tethys Ocean (Miller et al., 2003; Dubois-Côté et al., 2005). Obtaining a better understanding of the geodynamic evolution of the ophiolite in the Yarlung-Zangbo Suture Zone has long been highly prioritized by scholars due to its great significance in the reconstruction of the Tethys oceanic basin.

The Yarlung-Zangbo ophiolite belt is roughly distributed along the Yarlung-Zangbo River and is divided into three parts based on its spatial distribution: the eastern segment (Qushui-Motuo), the middle section (Angren-Renbu) and the western section (from the west of Saga to the Sino-India border) (Pan et al., 1997; Jiang et al., 2016). The western section can also be divided into a northern segment (Dajiweng-Saga) and a southern segment (Daba-Xiugugabu), where its structure and sequence are not fully exposed due to tectonic dismemberment. The Daba-Xiugugabu ophiolite belt is distributed in the NWW direction along the Daba-Purang-Xiugugabu, and it mainly includes ultramafic rocks, such as the Purang, Dongbo, Dangqiong and Xiugugabu rocks, and it is approximately 400 km long and 10 km to 35 km wide. These rocks are in fault contact with Late Triassic to Cretaceous marine carbonates, clastic rocks and mafic lava, or they are covered by Neogene-Quaternary deposits

* Corresponding author. E-mail: xuxiangzhensjl@aliyun.com

(Fig. 1, Xu et al., 2006).

As revealed by previous studies, the geologic characteristics of the Yarlung-Zangbo Suture Zone (Luo, 2019) are very sophisticated, and studies of the western section have revealed the multigenetic and multistage features of the different ophiolitic rock bodies (Qiu et al., 2005; Xu et al., 2006, 2008; Liu et al., 2010; Xu et al., 2011a; Feng et al., 2015; Li et al., 2015; She et al., 2017). There are also wide variations in the formation of the Daba-Xiugugabu ophiolite belt (Gansser, 1983; Searle et al., 1987; Guo et al., 1991; Pan et al., 1997; Miller et al., 2003; Huang et al., 2006; Bezard et al., 2011). A wide range of exotic minerals, alloys and native elements have been recovered from the Dangqiong peridotite, including diamonds (Xiong et al., 2016a). Thus, a multistage formation has been suggested for this body. Here, we performed detailed fieldwork on the Dangqiong rock mass of the Daba-Xiugugabu ophiolite belt, systematically collected samples of mantle peridotite and gabbro, and performed detailed mineral geochemical analyses to determine the tectonic environment of the ophiolite based on an in-depth analysis of the data obtained here.

2 Geological Setting

The Dangqiong ophiolite is located in the southern segment of the Yarlung-Zangbo Suture Zone, which is part of the Daba-Xiugugabu belt; the Purang rock mass is in contact with the North Himalaya fault zone to the south and in fault contact with the North Laangcuo block to the north. The Dangqiong mass is the largest in this region, and it occupies an area of approximately 700 km^2 in the western segment of the belt (Xiong et al., 2016a) and is distributed discontinuously, mostly as fresh outcrops that exhibit high degrees of serpentinization along the boundary faults with the surrounding rocks (Figs. 1–2).

The Dangqiong ophiolite is mainly composed of mantle peridotite, gabbro/diabase dykes, and siliceous rock. The mantle peridotite consists dominantly of harzburgite, with minor amount of dunite and locally lherzolite. The gabbro/diabase dykes are often intrusive and cut the mantle rocks, and they show distinctive late-stage formation features. Lenticular bodies and veins of chromitite are found in the dunite bands. The southern part of the rock mass is characterized by the development of gabbro and diabase dykes (Figs. 1–2). The dykes are usually tens of centimeters to several meters wide and a few meters to dozens of meters long, and they occur as veins and lenses in the mantle peridotite.

Thirty-five primary chromitite outcrop spots are found in the Dangqiong rock bodies, which are mostly distributed in dunite and harzburgite in the southern part of the rock mass. These ore bodies are mostly vein-shaped, although some are lenticular or irregular, and they mainly strike to the NE and NW.

3 Sampling and Analytical Methods

From a large collection of carefully selected mantle peridotite and gabbro samples, we obtained 47 polished thin sections. After a detailed petrographic examination was performed, eight thin sections were selected for electron microprobe analysis. These analyses were performed at the Key Laboratory of Nuclear Resources and the Environment (East China Institute of Technology), Ministry of Education, using a JEOL JXA-8100 electron microprobe with an Inca energy-dispersive spectrometer. The microprobe was operated at a voltage of 15 kV, a

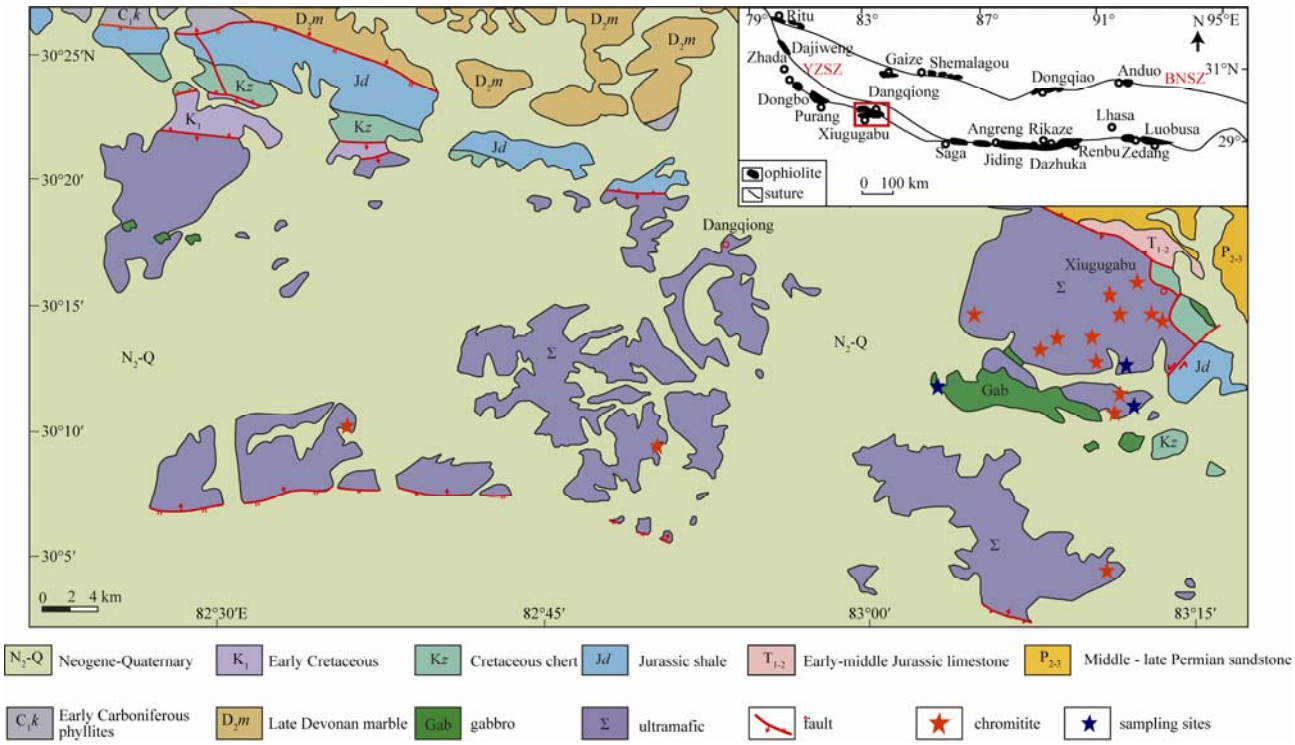

Fig. 1. Devonian of the Dangqiong ophiolite in the Yarlung-Zangbo Suture Zone (modified from Xiong et al., 2016a).

beam current of 20 amps and a spot diameter of 2 μm. A total of 40 olivine grains from four mantle peridotite samples (harzburgite and lherzolite) were analyzed, and their representative chemical compositions are shown in Table 1. For orthopyroxene, EPMA data were obtained from 23 points of four gabbro samples, 21 points of two lherzolite samples and nine points of two harzburgite samples. The representative results are shown in Table 2. For clinopyroxene, EPMA data were acquired from 31 points of four gabbro samples, 19 points from two lherzolite samples and 10 points from two harzburgite samples. The representative results are shown in Table 3. For chrome spinel, EPMA data were acquired from 19 points from 2 lherzolite samples and 30 points from 2

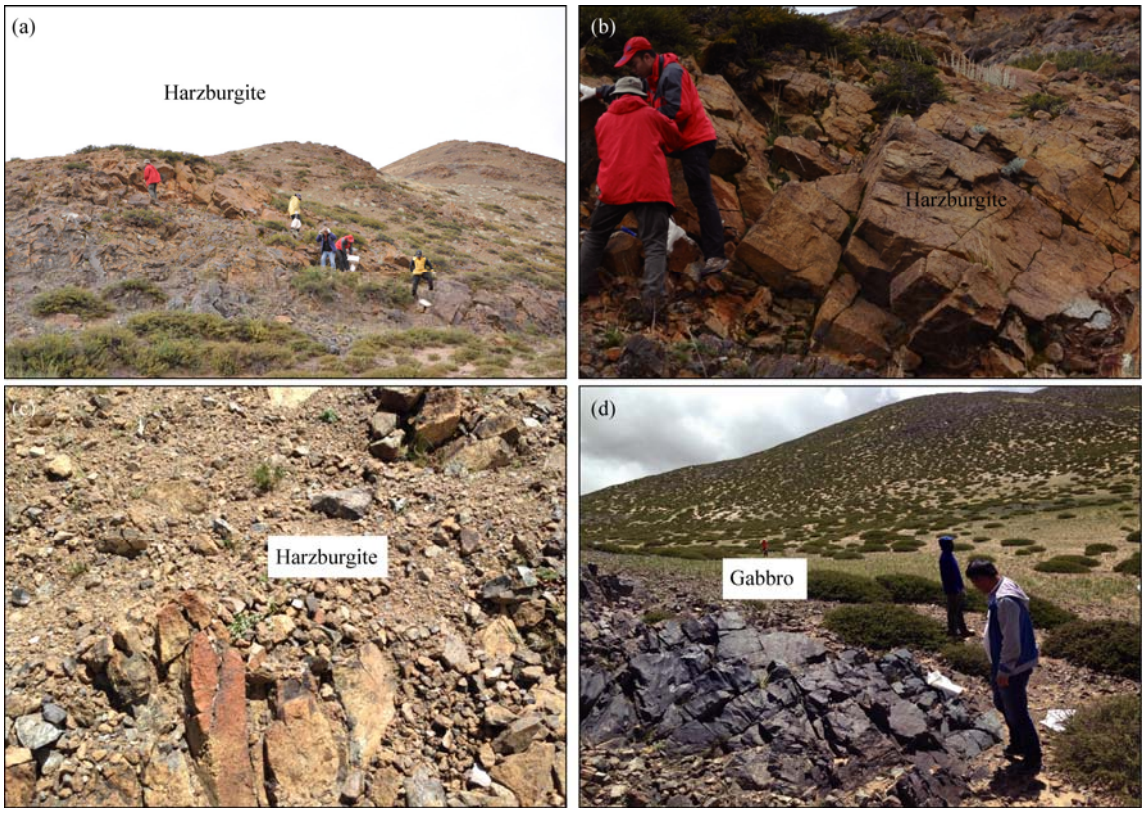

Fig. 2. Field photographs showing the mantle peridotite and gabbro in the Dangqiong ophiolite.
(a–c) Harzburgite in the Dangqiong ophiolite; (d) A gabbro vein in harzburgite.

Table 1 Representative microprobe analyses of olivine in the mantle peridotites of the Dangqiong ophiolite (wt%)

Lithology	Sample	Na_2O	NiO	K_2O	MgO	FeO	CaO	Al_2O_3	MnO	P_2O_5	SiO_2	Cr_2O_3	TiO_2	Total	Fo
Lherzolite	09y-588-12	0.00	0.41	0.00	48.65	8.72	0.01	0.03	0.15	0.00	40.86	0.11	0.00	98.94	90.87
	09y-588-16	0.00	0.44	0.01	48.38	9.41	0.01	0.00	0.09	0.00	41.12	0.10	0.00	99.55	90.16
	09y-588-18	0.02	0.38	0.00	47.98	9.43	0.00	0.00	0.13	0.00	40.92	0.16	0.01	99.03	90.07
	09y-588-24	0.00	0.42	0.00	47.90	9.42	0.01	0.00	0.13	0.00	41.27	0.04	0.00	99.19	90.06
	09y-588-32	0.00	0.40	0.00	47.98	9.20	0.00	0.00	0.14	0.01	41.02	0.03	0.05	98.82	90.29
	09y-593-25	0.00	0.38	0.01	48.81	8.68	0.01	0.01	0.13	0.01	40.84	0.12	0.00	99.00	90.93
	09y-593-27	0.01	0.40	0.00	49.83	8.53	0.00	0.01	0.12	0.00	41.45	0.08	0.01	100.44	91.24
	09y-593-29	0.00	0.39	0.00	48.31	9.20	0.01	0.00	0.11	0.03	40.42	0.05	0.02	98.55	90.35
	09y-593-40	0.00	0.35	0.01	48.94	8.92	0.01	0.00	0.12	0.00	41.11	0.00	0.01	99.46	90.72
	09y-593-42	0.00	0.41	0.00	48.24	9.22	0.00	0.00	0.14	0.02	40.50	0.22	0.03	98.77	90.32
Harzburgite	09y-616-4	0.00	0.36	0.01	48.81	9.40	0.01	0.00	0.13	0.00	40.99	0.00	0.00	99.70	90.25
	09y-616-6	0.00	0.41	0.01	49.07	9.46	0.00	0.00	0.15	0.00	40.78	0.04	0.00	99.93	90.24
	09y-616-16	0.00	0.34	0.02	49.13	9.27	0.00	0.00	0.08	0.00	41.39	0.05	0.00	100.28	90.43
	09y-616-18	0.04	0.40	0.00	47.42	9.47	0.01	0.00	0.12	0.04	40.38	0.06	0.01	97.96	89.92
	09y-616-20	0.00	0.41	0.01	48.48	9.15	0.00	0.00	0.13	0.02	41.24	0.05	0.01	99.49	90.42
	09y-616-24	0.00	0.37	0.01	48.72	9.44	0.01	0.00	0.13	0.02	41.08	0.17	0.03	99.98	90.20
	09y-616-33	0.00	0.37	0.00	48.53	9.48	0.02	0.00	0.11	0.01	41.04	0.06	0.01	99.62	90.13
	09y-617-5	0.02	0.40	0.02	47.85	7.80	0.05	0.32	0.11	0.00	40.98	0.05	0.02	97.61	91.63
	09y-617-10	0.01	0.38	0.00	48.85	9.04	0.03	0.01	0.17	0.00	41.05	0.05	0.03	99.60	90.59
	09y-617-21	0.02	0.42	0.01	48.36	9.39	0.05	0.01	0.13	0.02	40.85	0.03	0.00	99.29	90.18
	09y-617-34	0.03	0.43	0.00	48.80	9.18	0.02	0.00	0.18	0.02	41.14	0.15	0.00	99.93	90.45
	09y-617-36	0.00	0.46	0.00	49.39	8.20	0.03	0.18	0.09	0.00	41.50	0.14	0.00	99.99	91.48

Note: Fo = $100Mg/(Mg+Fe^{2+})$; and Fe^{2+} is total iron.

Table 2 Representative microprobe analyses of orthopyroxene in the gabbro and mantle peridotites of the Dangqiong ophiolite (wt%)

Lithology	Sample	Na_2O	NiO	K_2O	MgO	FeO	CaO	Al_2O_3	MnO	P_2O_5	SiO_2	Cr_2O_3	TiO_2	Total	En	Fs	Wo	$Mg^{\#}$
Gabbro	09y-688-1	0.00	0.00	0.00	21.15	23.93	1.06	0.69	0.64	0.00	52.90	0.03	0.14	100.53	59.86	37.99	2.15	61.17
	09y-688-4	0.04	0.00	0.00	20.20	23.76	1.13	0.66	0.67	0.00	52.66	0.01	0.17	99.29	58.82	38.82	2.36	60.24
	09y-686-2-5	0.03	0.00	0.00	19.50	25.35	1.17	0.72	0.77	0.03	52.78	0.00	0.19	100.53	56.42	41.16	2.42	57.82
	09y-686-2-9	0.03	0.00	0.00	20.70	23.42	1.05	0.75	0.69	0.00	53.78	0.01	0.18	100.60	59.84	37.98	2.18	61.17
	09y-689-6	0.01	0.01	0.00	21.32	22.78	0.79	0.55	0.68	0.03	51.90	0.03	0.16	98.26	61.51	36.85	1.64	62.53
	09y-689-10	0.02	0.03	0.02	21.54	21.70	1.15	0.68	0.59	0.00	52.20	0.01	0.13	98.06	62.37	35.25	2.39	63.89
	09y-689-14	0.02	0.00	0.00	21.36	22.87	0.98	0.71	0.66	0.00	52.35	0.00	0.17	99.11	61.21	36.77	2.01	62.47
	09y-687-6	0.01	0.02	0.00	21.17	24.12	1.13	0.76	0.62	0.01	52.66	0.04	0.18	100.70	59.60	38.11	2.29	61.00
Lherzolite	09y-588-6	0.00	0.10	0.00	34.18	6.30	0.63	3.29	0.18	0.02	55.53	0.79	0.04	101.06	89.56	9.25	1.19	90.64
	09y-588-9	0.01	0.12	0.01	34.74	6.18	0.54	3.32	0.11	0.00	55.68	0.78	0.01	101.48	90.03	8.98	1.00	90.93
	09y-588-10	0.04	0.05	0.01	34.31	6.30	0.65	3.38	0.11	0.00	55.29	0.75	0.01	100.90	89.56	9.22	1.23	90.67
	09y-588-22	0.00	0.10	0.00	35.62	6.23	0.34	1.53	0.15	0.02	57.22	0.24	0.04	101.47	90.50	8.87	0.62	91.07
	09y-588-28	0.02	0.10	0.00	33.10	6.52	0.40	1.72	0.20	0.01	56.51	0.21	0.03	98.80	89.36	9.87	0.77	90.06
	09y-593-2	0.00	0.11	0.00	31.66	6.75	0.55	4.82	0.22	0.00	54.21	1.00	0.02	99.34	88.34	10.56	1.10	89.32
	09y-593-10	0.00	0.06	0.01	31.22	6.50	0.88	4.99	0.16	0.00	54.12	1.05	0.02	99.00	87.96	10.27	1.78	89.55
	09y-593-23	0.01	0.09	0.01	33.07	6.17	0.67	2.81	0.09	0.01	56.21	0.44	0.03	99.60	89.35	9.35	1.30	90.52
Harzburgite	09y-616-3	0.03	0.05	0.01	32.20	6.00	1.40	3.22	0.09	0.00	55.85	0.58	0.01	99.45	88.05	9.20	2.75	90.54
	09y-616-35	0.00	0.05	0.01	35.36	6.22	0.69	2.83	0.12	0.01	56.72	0.49	0.05	102.54	89.88	8.87	1.25	91.02
	09y-617-2	0.00	0.06	0.00	33.99	6.49	0.25	1.61	0.15	0.00	55.65	0.26	0.05	98.49	89.91	9.62	0.47	90.33
	09y-617-8	0.02	0.04	0.01	34.40	6.25	0.66	3.05	0.15	0.03	55.84	0.57	0.01	101.01	89.62	9.14	1.24	90.74
	09y-617-18	0.00	0.08	0.00	32.55	6.70	0.42	3.01	0.11	0.02	55.17	0.35	0.03	98.42	88.91	10.26	0.83	89.65
	09y-617-23	0.01	0.09	0.01	33.01	6.31	0.48	3.61	0.14	0.00	55.68	0.59	0.05	99.98	89.47	9.59	0.93	90.32

Note: $Mg^{\#} = 100Mg/(Mg+Fe^{2+})$; and Fe^{2+} is total iron.

Table 3 Representative microprobe analyses of clinopyroxene in the gabbro and mantle peridotites of the Dangqiong ophiolite (wt%)

Lithology	Sample	Na_2O	NiO	K_2O	MgO	FeO	CaO	Al_2O_3	MnO	P_2O_5	SiO_2	Cr_2O_3	TiO_2	Total	En	Fs	Wo	$Mg^{\#}$
Gabbro	09y-688-3	0.32	0.00	0.00	14.96	12.60	17.96	1.33	0.33	0.00	52.54	0.05	0.25	100.33	42.83	20.23	36.94	67.93
	09y-688-5	0.34	0.00	0.00	14.18	9.61	20.99	1.50	0.31	0.00	52.59	0.05	0.29	99.86	40.90	15.56	43.54	72.44
	09y-688-11	0.27	0.04	0.01	14.99	12.10	18.05	1.38	0.30	0.01	52.88	0.03	0.30	100.37	43.14	19.53	37.33	68.84
	09y-686-2-22	0.27	0.02	0.00	14.63	10.30	20.77	0.87	0.33	0.04	53.41	0.01	0.19	100.85	41.41	16.36	42.24	71.69
	09y-686-2-24	0.25	0.00	0.00	14.70	8.93	21.84	1.31	0.29	0.01	53.29	0.00	0.25	100.86	41.51	14.15	44.34	74.58
	09y-687-5	0.25	0.00	0.04	14.73	14.11	16.22	1.82	0.36	0.01	51.86	0.00	0.27	99.67	42.95	23.07	33.98	65.06
	09y-687-9	0.27	0.01	0.00	14.51	9.96	20.59	1.40	0.32	0.01	52.42	0.03	0.34	99.85	41.58	16.01	42.42	72.20
	09y-687-11	0.26	0.00	0.02	13.82	9.77	21.17	1.32	0.30	0.04	52.99	0.00	0.31	100.00	40.04	15.87	44.08	71.61
Lherzolite	09y-588-2	0.14	0.05	0.00	16.95	2.50	22.58	3.59	0.08	0.04	52.18	1.05	0.11	99.26	49.02	4.06	46.92	92.35
	09y-588-13	0.04	0.08	0.00	18.19	2.16	23.35	1.71	0.07	0.01	54.51	0.30	0.01	100.42	50.26	3.35	46.38	93.74
	09y-588-17	0.07	0.04	0.00	18.29	2.17	23.28	1.50	0.04	0.00	53.85	0.27	0.10	99.60	50.47	3.36	46.17	93.76
	09y-593-13	0.14	0.04	0.00	18.24	2.81	20.78	4.39	0.09	0.00	52.41	1.26	0.09	100.24	52.50	4.53	42.97	92.06
	09y-593-14	0.19	0.06	0.01	16.72	2.35	22.74	4.63	0.10	0.00	51.88	1.40	0.08	100.15	48.63	3.83	47.55	92.70
	09y-593-15	0.17	0.05	0.00	16.56	2.21	22.86	4.64	0.10	0.02	51.98	1.32	0.10	100.01	48.38	3.62	48.00	93.04
	09y-593-17	0.15	0.04	0.01	16.46	2.13	22.88	4.46	0.11	0.00	52.13	1.34	0.08	99.79	48.28	3.50	48.22	93.25
	09y-593-20	0.13	0.05	0.00	16.72	2.25	22.91	4.66	0.14	0.06	51.86	1.30	0.07	100.15	48.54	3.67	47.79	92.98
	09y-593-38	0.14	0.01	0.00	17.19	2.02	23.06	3.19	0.11	0.00	52.78	0.79	0.10	99.39	49.27	3.24	47.49	93.82
Harzburgite	09y-616-1	0.26	0.07	0.00	17.33	2.30	23.06	3.89	0.09	0.00	52.79	1.05	0.10	100.92	49.25	3.66	47.09	93.09
	09y-616-27	0.21	0.04	0.00	18.20	2.32	22.63	2.20	0.09	0.00	53.84	0.49	0.04	100.05	50.88	3.64	45.47	93.32
	09y-617-6	0.11	0.04	0.00	17.95	2.02	23.08	2.11	0.06	0.03	53.34	0.47	0.12	99.33	50.31	3.18	46.51	94.06
	09y-617-15	0.19	0.05	0.00	17.40	2.35	22.62	3.72	0.07	0.02	52.83	0.75	0.16	100.16	49.74	3.77	46.48	92.95
	09y-617-19	0.20	0.03	0.01	16.93	2.28	21.89	3.59	0.09	0.01	51.37	3.09	0.14	99.63	49.87	3.77	46.36	92.98
	09y-617-22	0.16	0.02	0.00	17.76	1.83	23.48	2.33	0.06	0.01	53.70	0.56	0.13	100.04	49.80	2.88	47.32	94.53
	09y-617-26	0.18	0.01	0.00	17.64	2.30	23.28	3.03	0.06	0.02	53.30	0.41	0.11	100.33	49.46	3.62	46.93	93.18
	09y-617-29	0.19	0.09	0.00	18.22	2.39	22.94	2.08	0.06	0.00	54.08	0.43	0.07	100.54	50.54	3.72	45.74	93.15
	09y-617-38	0.16	0.04	0.00	17.42	1.99	23.67	2.62	0.10	0.00	55.07	0.46	0.11	101.64	49.00	3.14	47.86	93.98

Note: $Mg^{\#} = 100Mg/(Mg+Fe^{2+})$; and Fe^{2+} is total iron.

harzburgite samples. The representative results are shown in Table 4. EPMA data were also obtained from 14 feldspar points and 12 amphibole points from four gabbro samples, and these results are listed in Tables 5 and 6, respectively.

Nine mantle peridotite samples and eight gabbro samples were selected for whole-rock geochemical analysis. They were carefully cleaned, crushed and ground in an agate mortar to pass through a 200-mesh screen. The major element contents were determined on fused glass beads using X-ray fluorescence (XRF) spectrometry. The relative analytical accuracy was estimated to be 1% for SiO_2 and 2% for all other oxides. The contents of trace elements, including those of REEs, were determined using inductively coupled mass spectrometry (ICP-MS). Two national standard samples (GSR3 and GSR5) and three internal standards were measured simultaneously to ensure the consistency of the analytical results. The analytical uncertainties were estimated to be 10% for trace elements with abundances of <10 ppm and approximately 5% for those with abundances of >10 ppm.

Table 4 Representative microprobe analyses of chromite in the mantle peridotites of the Dangqiong ophiolite (wt%)

Lithology	Sample	Na_2O	NiO	K_2O	MgO	FeO	CaO	Al_2O_3	MnO	P_2O_5	SiO_2	Cr_2O_3	TiO_2	Total	$Mg^{\#}$	$Cr^{\#}$	$Fe^{2+,}$	Fe^{3+}
Lherzolite	09y-588-11	0.00	0.24	0.02	16.75	15.81	0.01	42.29	0.20	0.00	0.00	22.96	0.01	98.28	65.43	26.69	34.57	0.05
	09y-588-23	0.00	0.18	0.00	15.69	17.21	0.00	39.75	0.27	0.00	0.01	25.16	0.07	98.34	62.08	29.80	37.92	0.16
	09y-588-25	0.02	0.11	0.00	15.46	17.75	0.00	40.12	0.17	0.01	0.02	24.18	0.06	97.90	61.07	28.79	38.93	0.22
	09y-588-27	0.02	0.21	0.01	16.16	16.82	0.00	40.74	0.16	0.00	0.00	24.10	0.03	98.25	63.26	28.41	36.74	0.11
	09y-588-29	0.01	0.17	0.00	15.96	17.18	0.00	38.63	0.20	0.00	0.00	26.68	0.04	98.87	62.44	31.66	37.56	0.08
	09y-588-31	0.01	0.19	0.00	15.85	17.06	0.00	40.66	0.17	0.00	0.02	24.42	0.05	98.42	62.55	28.72	37.45	0.18
	09y-593-32	0.00	0.21	0.00	18.36	13.33	0.01	49.08	0.15	0.00	0.02	17.88	0.04	99.09	71.27	19.64	28.73	0.16
	09y-593-34	0.00	0.22	0.00	17.31	14.51	0.00	45.60	0.15	0.00	0.01	20.87	0.03	98.72	68.12	23.49	31.88	0.08
	09y-593-39	0.02	0.22	0.00	17.47	14.34	0.01	46.17	0.18	0.02	0.02	20.09	0.00	98.52	68.65	22.59	31.35	0.14
	09y-593-41	0.01	0.22	0.00	17.48	14.39	0.02	48.48	0.23	0.00	0.03	17.74	0.03	98.62	68.73	19.71	31.27	0.25
Harzburgite	09y-616-2	0.01	0.18	0.00	17.11	14.74	0.00	42.08	0.20	0.03	0.00	25.29	0.06	99.70	67.54	28.73	32.46	0.09
	09y-616-5	0.01	0.17	0.00	16.55	15.27	0.03	39.97	0.22	0.01	0.02	27.14	0.07	99.45	66.15	31.30	33.85	0.20
	09y-616-7	0.06	0.17	0.01	17.66	14.01	0.00	44.51	0.17	0.00	0.00	22.44	0.06	99.08	69.50	25.27	30.50	0.24
	09y-616-9	0.00	0.16	0.00	16.11	15.94	0.00	40.82	0.23	0.01	0.00	26.42	0.07	99.77	64.39	30.28	35.61	0.07
	09y-616-11	0.03	0.17	0.00	16.03	16.31	0.00	40.73	0.22	0.00	0.00	25.76	0.03	99.27	63.82	29.79	36.18	0.13
	09y-616-13	0.02	0.18	0.00	16.46	14.64	0.00	42.38	0.24	0.01	0.01	23.92	0.05	97.91	66.92	27.47	33.08	0.16
	09y-616-23	0.00	0.18	0.00	17.35	14.78	0.00	46.07	0.17	0.01	0.26	20.52	0.02	99.36	69.58	23.01	30.42	1.48
	09y-616-32	0.00	0.19	0.00	16.48	15.83	0.00	43.48	0.20	0.00	0.02	22.35	0.03	98.57	65.15	25.64	34.85	0.14
	09y-617-16	0.00	0.31	0.00	18.98	12.89	0.03	49.78	0.13	0.00	0.01	17.34	0.04	99.50	72.52	18.94	27.48	0.08
	09y-617-20	0.00	0.29	0.00	17.94	13.90	0.00	47.17	0.16	0.01	0.00	19.76	0.09	99.33	69.83	21.94	30.17	0.10
	09y-617-33	0.06	0.32	0.01	18.43	13.96	0.02	50.66	0.13	0.00	0.01	16.21	0.02	99.83	70.47	17.67	29.53	0.23
	09y-617-35	0.01	0.23	0.01	18.09	13.56	0.00	49.06	0.19	0.02	0.00	18.02	0.03	99.22	70.50	19.77	29.50	0.08

Note: $Fe^{2+,} = 100Fe^{2+}/(Mg+Fe^{2+})$, $Mg^{\#} = 100Mg/(Mg+Fe^{2+})$, $Cr^{\#} = 100Cr/(Cr+Al)$, $Fe^{3+,} = 100Fe^{3+}/(Cr+Al+Fe^{3+})$.

Table 5 Representative microprobe analyses of feldspar in the gabbros of the Dangqiong ophiolite (wt%)

Sample	Na_2O	NiO	K_2O	MgO	FeO	CaO	Al_2O_3	MnO	P2O5	SiO_2	Cr_2O_3	TiO_2	Total	Ab	An	Or
09y-686-2-12	5.29	0.01	0.03	0.00	0.24	11.12	29.45	0.00	0.03	54.79	0.00	0.03	100.98	46.2	53.7	0.2
09y-686-2-21	5.10	0.00	0.01	0.01	0.12	11.44	29.19	0.00	0.03	54.44	0.00	0.00	100.35	44.6	55.3	0.1
09y-686-2-23	5.18	0.00	0.02	0.03	0.22	11.38	29.13	0.00	0.00	54.69	0.00	0.00	100.64	45.1	54.8	0.1
09y-689-8	5.17	0.02	0.02	0.03	0.16	10.84	28.23	0.02	0.00	53.60	0.01	0.03	98.14	46.3	53.6	0.1
09y-689-11	4.99	0.00	0.01	0.02	0.12	11.02	29.14	0.00	0.02	53.39	0.02	0.04	98.78	45.0	55.0	0.0
09y-689-13	5.15	0.00	0.01	0.01	0.18	10.72	28.41	0.03	0.02	54.29	0.02	0.01	98.85	46.5	53.5	0.0
09y-687-3	5.23	0.00	0.03	0.03	0.12	11.11	28.93	0.00	0.00	55.12	0.05	0.00	100.63	45.9	53.9	0.2
09y-687-18	4.87	0.03	0.01	0.00	0.15	11.40	29.38	0.00	0.00	54.29	0.00	0.03	100.16	43.6	56.4	0.0
09y-687-19	5.01	0.03	0.02	0.00	0.11	11.57	29.37	0.00	0.00	54.46	0.00	0.02	100.59	43.9	56.0	0.1
09y-687-21	4.88	0.00	0.03	0.02	0.15	11.77	29.54	0.00	0.00	53.99	0.04	0.03	100.46	42.8	57.0	0.2
09y-687-25	4.91	0.00	0.02	0.03	0.19	11.53	29.36	0.00	0.00	53.82	0.00	0.00	99.86	43.5	56.4	0.1
09y-687-27	5.24	0.00	0.04	0.00	0.16	10.59	29.16	0.00	0.01	56.22	0.01	0.02	101.44	47.1	52.7	0.2
09y-687-28	4.82	0.01	0.00	0.03	0.13	11.69	29.45	0.02	0.00	53.85	0.01	0.03	100.03	42.7	57.3	0.0
09y-687-29	4.92	0.01	0.03	0.01	0.09	11.39	29.23	0.00	0.03	54.41	0.02	0.01	100.14	43.8	56.0	0.2

Table 6 Representative microprobe analyses of amphiboles in the gabbros of the Dangqiong ophiolite (wt%)

Sample	Na_2O	NiO	K_2O	MgO	FeO	CaO	Al_2O_3	MnO	P_2O_5	SiO_2	Cr_2O_3	TiO_2	Total	Mg/Mg+Fe
09y-688-2	2.29	0.00	0.06	13.13	14.23	10.59	9.86	0.19	0.04	45.17	0.02	2.50	98.07	0.62
09y-688-9	1.86	0.00	0.05	14.09	13.52	11.92	7.20	0.20	0.03	47.57	0.03	1.87	98.34	0.65
09y-686-2-2	2.24	0.00	0.07	13.58	14.49	10.70	9.66	0.23	0.02	45.38	0.00	2.15	98.52	0.63
09y-686-2-4	2.36	0.00	0.08	13.16	14.37	10.99	10.02	0.18	0.05	45.36	0.01	2.55	99.11	0.62
09y-686-2-14	1.70	0.00	0.08	15.02	13.14	11.16	8.22	0.17	0.01	48.19	0.03	1.34	99.06	0.67
09y-689-7	2.25	0.00	0.07	13.39	13.15	10.33	9.53	0.17	0.01	44.51	0.01	2.23	95.65	0.65
09y-689-12	2.30	0.04	0.11	13.24	13.48	10.54	9.58	0.18	0.01	44.45	0.00	2.44	96.36	0.64
09y-687-4	2.02	0.00	0.07	13.29	13.15	10.98	9.72	0.17	0.03	45.17	0.07	2.72	97.38	0.64
09y-687-8	1.58	0.03	0.09	15.32	13.10	11.04	7.65	0.15	0.01	48.00	0.00	1.10	98.07	0.68
09y-687-13	2.34	0.01	0.08	13.59	13.40	11.16	9.60	0.15	0.00	45.27	0.02	2.41	98.01	0.64
09y-687-20	2.16	0.03	0.08	13.86	13.64	11.19	8.93	0.18	0.04	46.26	0.03	2.02	98.42	0.64
09y-687-23	2.22	0.03	0.07	12.41	17.52	9.86	10.57	0.21	0.00	43.06	0.04	1.89	97.87	0.56

4 Discussion

4.1 Petrologic features

Harzburgite is fresh and mostly olive green or ink green, and the weathering surface is mostly brown or yellow and features visible orthopyroxene granules (Fig. 2). The harzburgite exhibits granular and massive structures, and it consists mainly of olivine and orthopyroxene, as well as a small amount of clinopyroxene, and the most common accessory mineral is chromite. Serpentinization is widely developed and mainly occurs on the surface or along fractures or fault surfaces.

Harzburgite consists of olivine (75%–80%), orthopyroxene (mainly enstatite, 15%–20%), clinopyroxene (mainly diopside, 5%), and approximately 1%–2% accessory minerals, such as chromite (chrome spinel) and magnetite. The alteration minerals include serpentine, brucite, magnesite, and chlorite. Olivine is granular and shows distinctive stress deformation features, such as recrystallization, kink banding and wavy extinction (Fig. 3a). Fine-grained olivine can be seen in the shear zone and exhibits irregular, subhedral-euhedral granular textures

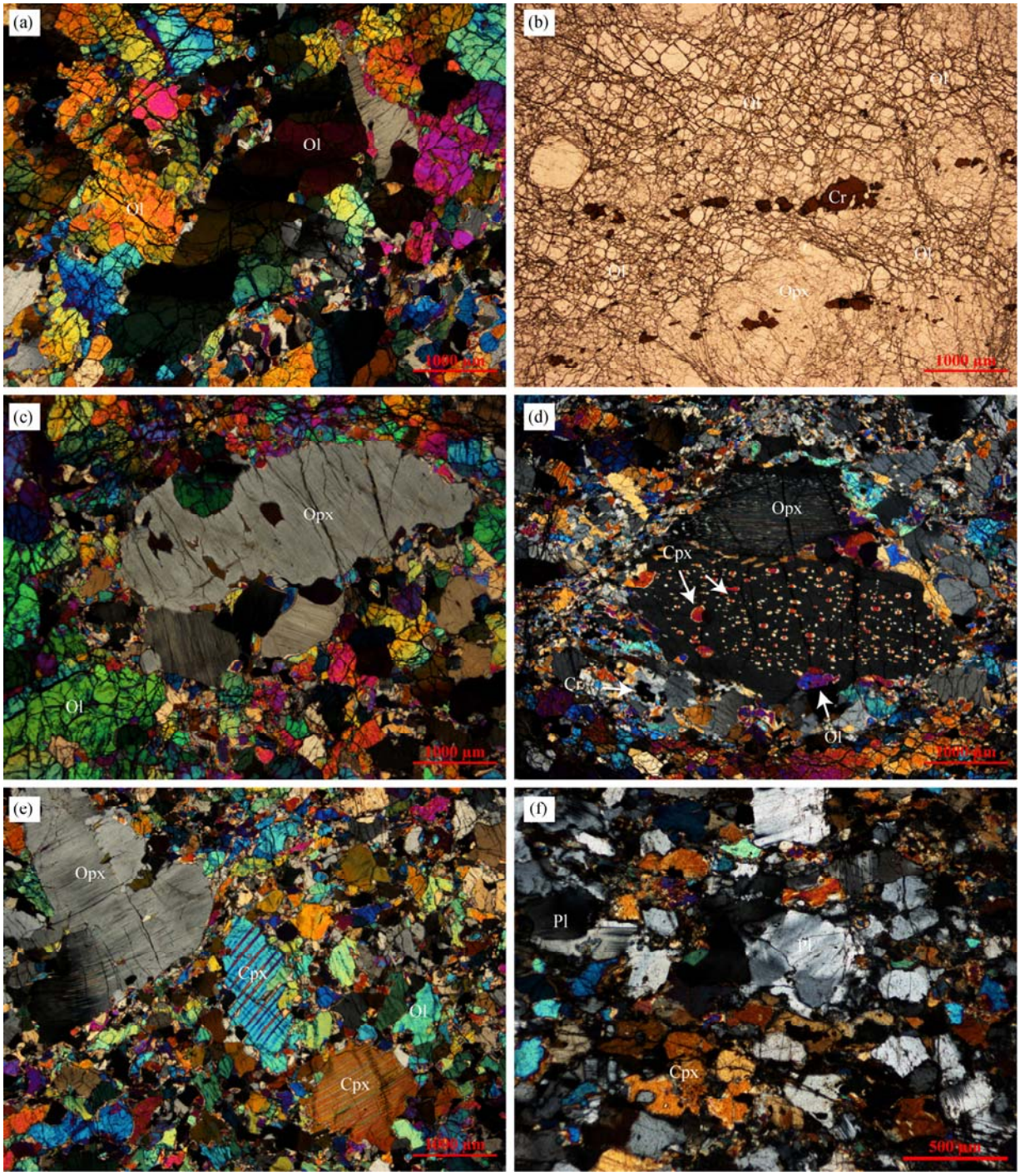

Fig. 3. Microphotographs of mantle peridotite and gabbro in the Dangqiong ophiolite.
(a) Wavy extinction of olivine (harzburgite, crossed polarizer); (b) recrystallized thin olivine, orientated chrome spinel (harzburgite, polarizer); (c) crystal deflection of orthopyroxene under stress (harzburgite, crossed polarizer); (d) A large number of parallel clinopyroxene exsolution are found in orthopyroxene, aligned (harzburgite, crossed polarizer); (e) large clinopyxene grains with obvious twisting deformation (lherzolite, crossed polarizer); (f) euhedral-semieuhedral granular pyroxene filling in a plagioclase framework and a typical gabbro texture (gabbro, crossed polarizer).

and recrystallization textures (Fig. 3b). The stress deformation features of orthopyroxene include crystal deflection, wavy extinction and glide twinning (Fig. 3c). There are abundant instances of parallel-extinct clinopyroxene exsolution in the orientated arrangement (Fig. 3d), while individual clinopyroxene grains are xenomorphic-subhedral in shape. The accessory mineral chromite is mainly subhedral, rare and heterogeneous, and it occurs scattered within olivine (Fig. 3b).

Clinopyroxene in the lherzolite is granular, approximately 1 mm in size and unoriented, and it is distributed within olivine with a content of 5%–10% (Fig. 3e). The orthopyroxene grains are columnar, xenomorphic and granular, with a content of 10%; they exhibit abundant

parallel, thin clinopyroxene exsolutions, as well as apparent deformation features and wavy extinction under the orthogonal polarizer (Fig. 3e). The olivine grains are granular and cracked, and they exhibit slight serpentinization. The small olivine crystals are banded, with a content of 70%–80%.

Gabbro is very fresh and greenish, with gabbroic texture and massive structure (Fig. 2d); gabbro mainly comprises 50% –55% plagioclase, 30% –40% pyroxene, 0–5% amphibole, and minor magnetite and other dark minerals. Plagioclase comprises euhedral-subhedral platy grains ranging in size from 0.2–0.5 mm, which are disorderly in their distribution and exhibiting polycrystalline twinning and high degrees of sericitization and zoisitization. Pyroxene is euhedral-subhedral and approximately 0.1 mm in size, and it fills in the plagioclase framework with a typical gabbro texture (Fig. 3f).

4.2 Mineral chemistry

4.2.1 Olivine

The EPMA results indicate that the olivine is forsterite, with Fo contents ranging from 89.92–91.63. No dunite was detected in this study. The olivine compositions in lherzolite and harzburgite are similar, with Fo contents ranging from 90.06–91.24 and 89.92–91.63, respectively.

Olivine contains a certain amount of NiO. Table 1 and Fig. 4 show that the NiO contents in olivine are similar in both the lherzolite and harzburgite, with an average value of 0.4%. The Cr_2O_3 contents in the olivine crystals are very low and range from 0.00%–0.22% and 0.00%–0.17% in the lherzolite and harzburgite, respectively.

4.2.2 Orthopyroxene

The orthopyroxene composition in the Dangqiong mantle peridotite is very homogeneous. The orthopyroxene in lherzolite is mainly enstatite, with $Mg^{\#}$ values of 89.32–91.07, and the En component is 87.96%–90.50%, with an average value of 89.22% (Fig. 5a). The orthopyroxene in harzburgite has $Mg^{\#}$ values of 89.65–91.02, and the En component is 88.05%–89.91%, with an average value of 89.29%. The orthopyroxene in gabbro is hypersthene, with $Mg^{\#}$ values of 57.82–63.89, and the En component is 56.42%–62.37%, with an average value of 59.59%. The orthopyroxene in the mantle peridotite has more Mg than that in the gabbro (Fig. 5b).

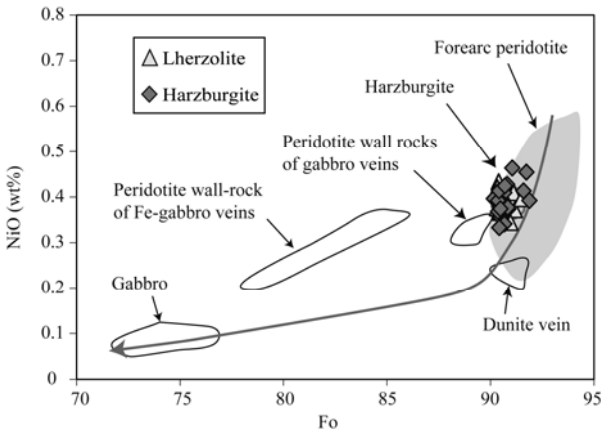

Fig. 4. NiO vs Fo contents of olivine in the different lithologies of the Dangqiong ophiolite.

Fields outline the olivine compositions in forearc peridotites (Ishii et al., 1992) and various mantle peridotites, ultramafic and mafic plutonic rocks from the oceanic domain (Constantin et al., 1995). The arrow is compatible with the fractional crystallization trend (Constantin, 1999).

The orthopyroxenes in different types of rocks generally record low NiO contents (wt%) of 0.00%–0.12% and Cr_2O_3 contents of 0.00%–1.05%. The Al_2O_3 content varies dramatically and is closely related to the lithofacies; in the gabbro, the Al_2O_3 content is as low as 0.55%–0.76%, with an average value of 0.69%; in the harzburgite, it ranges from 1.61%–3.61%, with an average value of 2.78%; and in the lherzolite, it ranges from 1.53%–4.99%, with an average value of 3.68%.

The Al_2O_3 content in orthopyroxene can be used as an index of the degree of partial melting (Dick, 1977). It is generally believed that lower Al_2O_3 contents in the orthopyroxene in the mantle peridotite of the ophiolite correspond to a greater degree of melting, and based on this criterion, the low Al_2O_3 contents and high $Mg^{\#}$ values of the samples imply that the mantle peridotite in this area has experienced a high degree of partial melting (Dick and Bullen, 1984). As shown in Fig. 5b, the Al_2O_3 contents of the orthopyroxene in the harzburgite are lower than those in the lherzolite, which also demonstrates that as the degree of partial melting increases, the Al_2O_3 content decreases (Dick and Natland, 1996).

4.2.3 Clinopyroxene

Clinopyroxene occurs in various lithologies, with its content varying greatly (Fig. 5c–d). The clinopyroxene in the gabbro (En_{40-43}, Wo_{34-44}, Fs_{14-23}) is dominant augite. This clinopyroxene has $Mg^{\#}$ values ranging from 65.06–74.58, with an average value of 71.41; Cr_2O_3 contents ranging from 0 to 0.05 wt% (Fig. 5d); and Al_2O_3 and TiO_2 contents ranging from 0.87 wt% to 1.82 wt% and 0.19 wt% to 0.34 wt%, respectively.

Clinopyroxenes from the mantle peridotite (and even the exsolution lamellae in orthopyroxene) are compositionally defined as diopside (lherzolite: En_{48-53}, Wo_{43-48}, Fs_{3-5}; harzburgite: En_{49-51}, Wo_{45-48}, Fs_{3-4}) (Fig. 5c). The clinopyroxenes in the lherzolites have $Mg^{\#}$ values ranging from 92.06–93.82, with an average value of 92.97; Cr_2O_3 contents ranging from 0.27 wt%–1.4 wt% (Fig. 5d); and Al_2O_3 and TiO_2 contents ranging from 1.5 wt%–4.66 wt% and 0.01 wt%–0.11 wt%, respectively. The clinopyroxenes in the harzburgites have $Mg^{\#}$ values ranging from 92.95–94.53, with an average value of 93.43; Cr_2O_3 contents ranging from 0.41 wt%–3.09 wt% (Fig. 5d); and Al_2O_3 and TiO_2 contents ranging from 2.08 wt%–3.89 wt% and 0.04 wt%–0.16 wt%, respectively.

The analysis results of all the clinopyroxenes indicate that they also follow the main oceanic tholeiitic fractional crystallization trend of Constantin (1999).

4.2.4 Chrome spinel

Chrome spinel has been found in all the samples, with a very low content (generally, less than 5 wt%). The type of chrome spinel is greatly dependent on the proportions of the two main trivalent oxides, Cr_2O_3 and Al_2O_3. Based on the EPMA data, the chrome spinels in lherzolite have

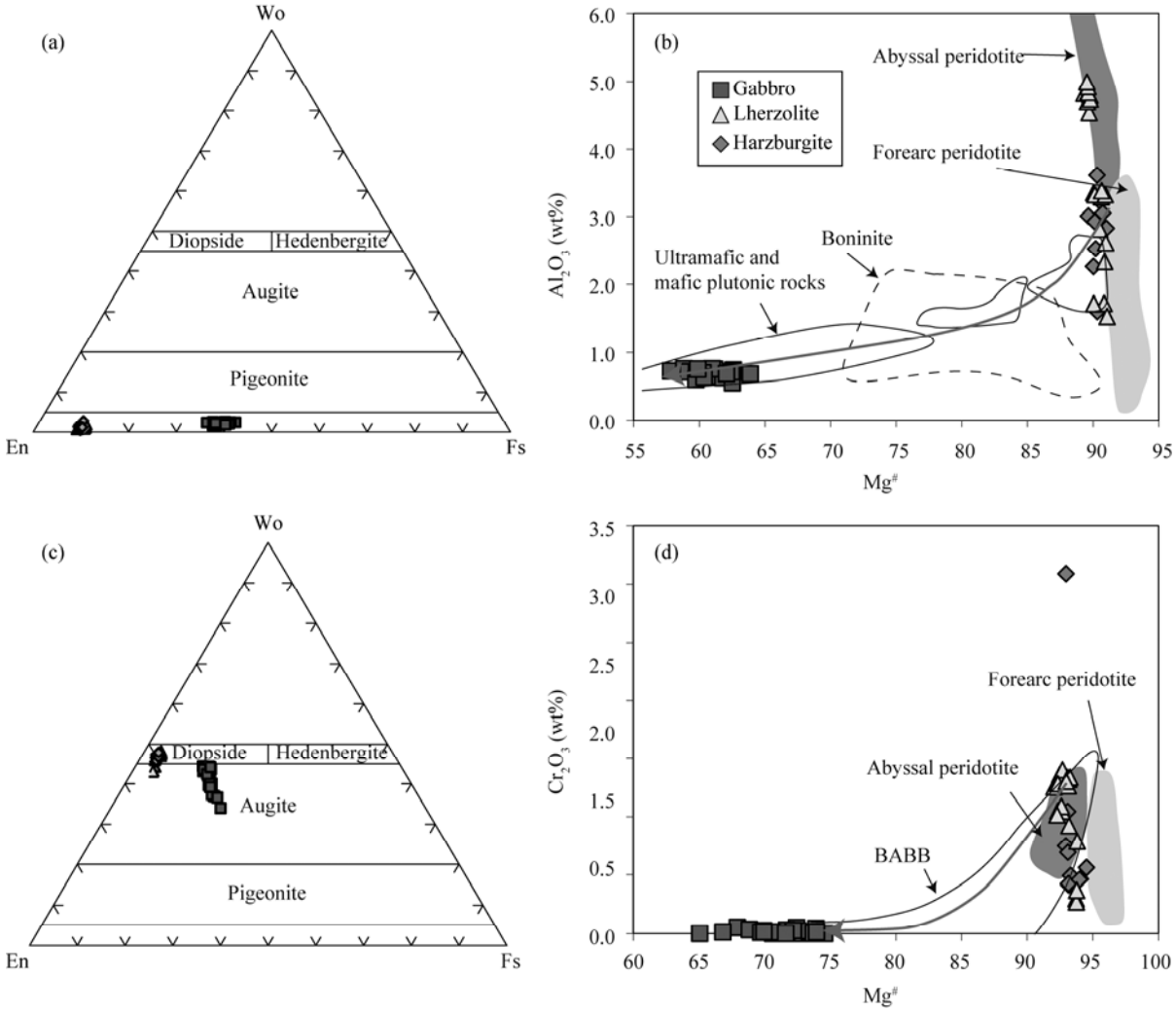

Fig. 5. Pyroxene compositions in the different lithologies of the Dangqiong district.

(a) Wo-En-Fs (after Morimoto (1988); (b) $Mg^{\#}$ vs. Al_2O_3 (wt%); (c) Wo-En-Fs (after Morimoto (1988); (d) $Mg^{\#}$ vs. Cr_2O_3 (wt%).
Fields outline orthopyroxene compositions in abyssal peridotites (Johnson et al., 1990), forearc peridotites (Ishii et al., 1992), boninites (Van der Laan et al., 1992), back-arc-basin basalt (BABB) field from Hawkins and Allan (1994), and ultramafic and mafic plutonic rocks from Pito, Terevaka and Garrett (Constantin, 1999).

Cr_2O_3 contents of 17.74 wt%–26.68 wt%, with an average value of 22.26 wt%; Al_2O_3 contents of 38.63 wt%–49.08 wt%, with an average value of 43.58 wt%; $Cr^{\#}$ values of 19.64–31.66; and $Mg^{\#}$ values of 61.07–71.27. The chrome spinels in harzburgite have Cr_2O_3 contents of 16.21 wt%–27.14 wt%, with an average value of 21.22 wt%; Al_2O_3 contents of 39.97 wt%–50.66 wt%, with an average value of 45.44 wt%; $Cr^{\#}$ values of 17.67–31.3; and $Mg^{\#}$ values of 63.82–72.52. Both types of chrome spinel contain very low TiO_2 contents (0–0.09 wt%). Calculations were performed using that of Hirose and Kawamoto (1995; Fig. 6), and the results indicate that the Dangqiong chrome spinels reflect only a low degree of partial melting (10–15 wt%).

The formation of a spinel is controlled by the degree of melting and the formation pressure of the mantle peridotite (Dick and Bullen, 1984). The $Cr^{\#}$ of spinel and $Mg^{\#}$ of olivine can be used to determine the degree of partial melting, formation pressure and tectonic environment of their host rocks (Pearce et al., 2000). As an accessory mineral, the chemical composition of chrome spinel is an indicator of the chemical composition of its host rock, i.e., mantle peridotite. The chemical compositions and $Cr^{\#}$-$Mg^{\#}$ diagram (Fig. 6) reveal that the $Cr^{\#}$ and $Mg^{\#}$ values have a negative correlation, similar to those observed in most Alps-type ultramafic rocks around the world; that is, the $Cr^{\#}$ value decreases as the $Mg^{\#}$ value increases (Leblance, 1980), and the formation environments of the harzburgite and lherzolite are similar to that of abyssal peridotite.

4.2.5 Feldspar

The feldspar in gabbro samples is plagioclase (An_{43-47}, Ab_{53-57}) (Table 5). The feldspar composition reflects low-temperature re-equilibration. The gabbro samples contain plagioclase that most likely retained its magmatic composition.

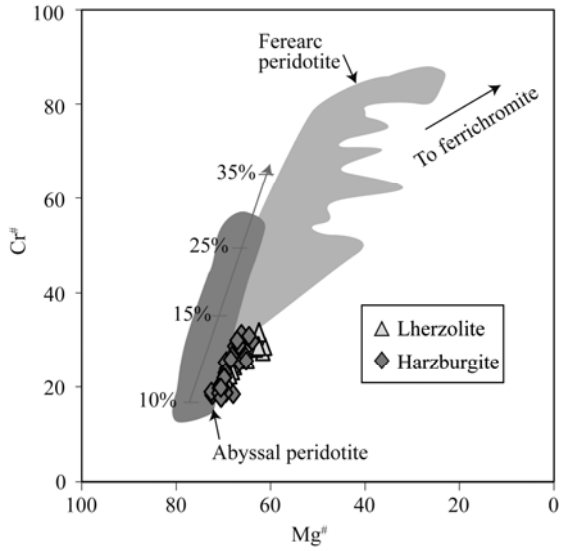

Fig. 6. Chrome spinel composition in the Dangqiong peridotites.
Fields for the spinels in abyssal peridotites are taken from Dick and Bullen (1984). Data for spinel in forearc peridotites are from Ishii et al. (1992) and Parkinson and Pearce (1998). The curve with ticks represents the experimental percentage of wet melting of the host peridotites (Hirose and Kawamoto, 1995).

4.2.6 Amphibole

Only metamorphic amphiboles were analyzed in the gabbro samples collected from the Dangqiong massif. According to the classification of Leake et al. (1997, 2004), these metamorphic amphiboles are mainly magnesio-amphibole (Fig. 7, Table 6), with $Mg^{\#}$ values ranging from 0.56 to 0.68, and they have high TiO_2 and Al_2O_3 contents (1.1 wt%–2.72 wt% and 7.2 wt%–10.57 wt%, respectively).

Based on previous research of metasomatic amphiboles from mantle xenoliths in different tectonic environments, the amphiboles in the upper mantle wedge xenoliths from subduction zones have higher SiO_2 contents and lower Na_2O and TiO_2 contents than those from intraplate environments (Coltorti et al., 2007). Figure 7b indicates that the amphibole from the Dangqiong area formed in a subduction zone environment.

4.3 Whole-rock chemistry

4.3.1 Mantle peridotite

Whole-rock geochemical analyses were performed on nine samples, including two lherzolites and seven harzburgites (Table 7). All of the peridotites in Dangqiong are very fresh, with LOI contents that typically <1 wt%. The Al_2O_3 and CaO contents in the harzburgites are 0.96–1.72 (wt%) and 0.71–2.5 (wt%) respectively, which are similar to those in the lherzolites. All samples are all Mg-rich (average MgO=42.45 wt%), Al-poor (average Al_2O_3=1.37 wt%), and alkali-poor (most Na_2O < 0.01 wt%; K_2O < 0.01 wt%).

The MgO content in mantle peridotite represents an index of mantle depletion or partial melting. Higher contents of MgO together with lower contents of CaO, Al_2O_3 and SiO_2 indicate higher degrees of melting (Coleman, 1977; Nicolas and Prinzhofer, 1983; Hartmann and Wedepohl, 1993). Petrologically, during the melting process of basaltic magma from the upper mantle, fusible components such as CaO, Al_2O_3, and SiO_2 tend to enter the melt. As more basaltic magma melts out, the residual mantle peridotite becomes richer in MgO and the mantle becomes more depleted. The MgO content of the mantle peridotite in the Dangqiong belt (Table 7, Fig. 8) is much higher than that of the primitive mantle, despite the slight difference in their degree of melting, indicating that the ophiolite belt cropping out in the Dangqiong area has undergone a higher degree of mantle depletion or partial melting and is very similar to the ophiolite in Bangonghu, Shiquanhe and the western Yarlung-Zangbo Suture Zone (Qiu et al., 2005). Most of the elements in peridotite have a good negative correlation with the MgO content. The contents of incompatible elements, such as Al_2O_3, CaO and SiO_2, are negatively correlated with the MgO content (Fig. 8). Compared to the abyssal mantle peridotite (or MOR-type mantle peridotite) and subduction mantle peridotite (or SSZ-type mantle peridotite), the compositions of the lherzolite and some harzburgite samples are similar to that of abyssal mantle peridotite, and two harzburgite samples fall in the subduction mantle

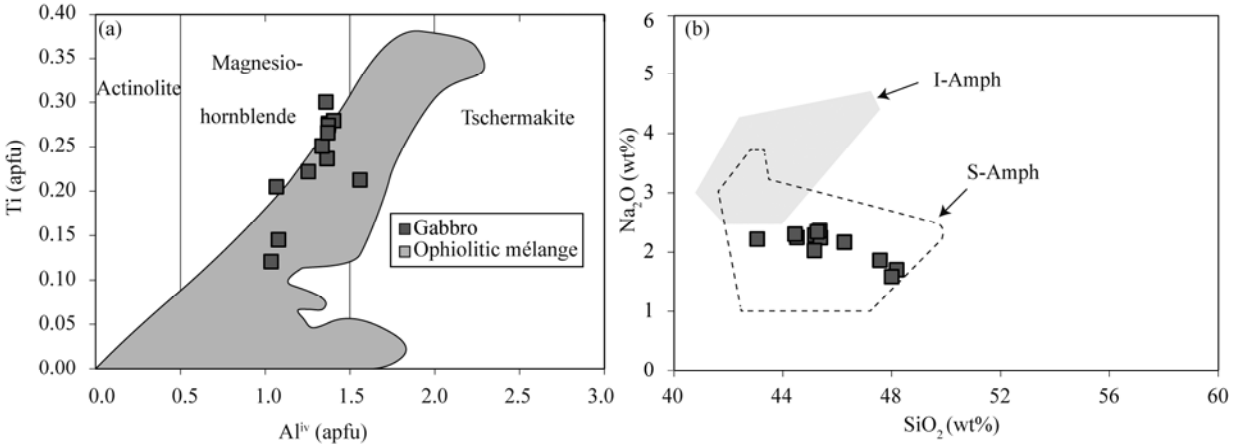

Fig. 7. Diagram of amphibole (Amp) in the Dangqiong gabbro.
(a) Variations of Al^{4+} vs. Ti (apfu), the field for the ophiolitic mélange is from Dupuis et al. (2005) , Huot et al. (2002) and Coltorti (2004); (b) Plot of SiO_2 vs. Na_2O. I-Amph, amphibole in intra plate environment including the intra continental, oceanic island and ocean ridge. S-Amph, amphibole in subduction environment, mainly the upper mantle wedge (Coltorti et al., 2007).

Table 7 Major and trace element compositions of the whole-rock samples of peridotite and gabbro of the Dangqiong ophiolite

Lithology	Lherzolite				Harzburgite								Gabbro				
Sample	09y-588	09y-593	09y-584	09y-585	09y-586	09y-592	09y-594	09y-595	09y-596	09y-680	09y-681	09y-682	09y-683	09y-684	09y-685	09y-686	09y-687
Major element (wt%)																	
SiO_2	44.25	46.00	45.82	43.26	44.4	45.06	44.23	43.58	45.92	47.36	41.89	46.51	48.48	46.8	44.07	44.57	46.38
Al_2O_3	1.25	1.66	1.72	1.03	1.59	1.41	0.99	0.96	1.68	15.3	16.2	15.1	15.87	14.83	14.84	15.04	15.15
Fe_2O_3	2	1.44	3.34	0.91	1.7	1.5	1.74	2.15	2.39	3.31	2.53	4.07	3.66	3.97	3.39	3.65	3.34
FeO	6.45	6.76	5.12	7.98	6.66	6.92	6.83	6.05	5.73	7.46	4.62	6.72	7.33	6.77	6.99	7.15	7.4
CaO	1.59	1.86	1.99	1.3	2.5	1.58	0.71	0.84	2.08	12.24	15.5	13.37	11.77	12.57	15.27	14.57	12.82
MgO	41.88	41.08	40.73	44.18	40.6	42.78	44.98	44.37	41.43	7.62	11.95	7.51	7.74	7.34	7.72	7.81	7.9
K_2O	<0.01	<0.01	<0.01	<0.01	<0.01	<0.01	<0.01	<0.01	<0.01	0.03	0.04	0.02	0.03	0.04	0.02	0.02	0.02
Na_2O	0.06	<0.01	0.01	<0.01	0.01	<0.01	0.12	0.02	<0.01	2.27	0.71	1.79	2.53	2.56	1.21	1.46	1.96
TiO_2	0.01	0.02	0.01	<0.01	0.01	0.01	0.01	0.01	0.01	1.36	1.28	1.34	1.39	1.34	1.34	1.38	1.36
MnO	0.14	0.14	0.14	0.14	0.14	0.14	0.13	0.12	0.14	0.2	0.13	0.21	0.2	0.2	0.19	0.2	0.2
P_2O_5	<0.01	<0.01	0.01	<0.01	<0.01	<0.01	<0.01	<0.01	<0.01	0.1	0.1	0.1	0.1	0.1	0.09	0.1	0.1
H_2O+	1.5	0.12	0.6	0.6	1.28	0.3	0.3	0.92	0.22	1.88	4.5	2.7	0.68	2.74	4.02	3.4	2.58
CO_2	0.12	0.12	0.12	0.12	0.21	0.21	0.12	0.21	0.12	0.39	0.21	0.3	0.3	0.12	0.21	0.21	0.12
LOI	0.94	-0.35	0.13	0.01	0.7	-0.29	-0.29	0.34	-0.23	1.29	4.48	2.16	0.28	2.3	3.44	2.87	1.91
Total	97.63	98.96	98.89	98.8	97.61	99.4	99.74	98.1	99.38	97.25	94.95	96.74	99.1	96.52	95.13	95.95	96.63
$Mg^{\#}$																	
Trace element (ppm)																	
La	0.02	0.17	0.19	0.03	0.04	0.12	0.10	0.15	0.14	1.59	2.89	1.64	1.68	1.64	1.49	1.62	1.51
Ce	0.04	0.24	0.37	0.06	0.08	0.04	0.06	0.06	0.24	6.23	9.88	6.11	6.28	6.00	5.67	6.02	5.84
Pr	0.00	0.03	0.04	0.01	0.01	0.02	0.02	0.03	0.03	1.25	1.75	1.22	1.28	1.22	1.13	1.23	1.23
Nd	0.02	0.11	0.16	0.02	0.04	0.10	0.05	0.14	0.09	7.28	9.20	7.01	7.35	7.08	6.91	7.11	6.90
Sm	0.00	0.02	0.04	0.01	0.00	0.02	0.01	0.04	0.02	2.79	3.09	2.71	2.83	2.87	2.70	2.81	2.70
Eu	0.00	0.01	0.01	0.00	0.00	0.00	0.00	0.01	0.01	1.15	1.23	1.09	1.09	1.14	1.11	1.13	1.07
Gd	0.04	0.06	0.08	0.03	0.04	0.03	0.02	0.04	0.03	4.22	4.63	4.20	4.13	4.11	4.00	4.09	4.18
Tb	0.01	0.01	0.01	0.01	0.01	0.01	0.00	0.01	0.01	0.77	0.83	0.75	0.77	0.75	0.72	0.75	0.75
Dy	0.06	0.09	0.13	0.06	0.12	0.07	0.05	0.07	0.09	5.32	5.66	5.10	5.29	5.10	5.12	5.18	4.99
Ho	0.02	0.02	0.03	0.02	0.03	0.02	0.01	0.01	0.03	1.15	1.26	1.08	1.13	1.11	1.09	1.13	1.11
Er	0.06	0.09	0.10	0.06	0.10	0.06	0.04	0.05	0.09	3.35	3.63	3.08	3.26	3.21	3.13	3.27	3.16
Tm	0.01	0.02	0.02	0.01	0.01	0.01	0.01	0.01	0.02	0.46	0.51	0.44	0.47	0.46	0.46	0.46	0.45
Yb	0.10	0.12	0.13	0.08	0.13	0.10	0.06	0.06	0.11	3.05	3.44	2.88	2.93	2.90	2.83	2.94	2.97
Lu	0.02	0.02	0.02	0.01	0.02	0.02	0.01	0.01	0.02	0.44	0.48	0.42	0.44	0.43	0.40	0.41	0.41
∑REE	0.39	0.99	1.31	0.41	0.63	0.61	0.44	0.68	0.92	39.04	48.50	37.73	38.93	38.00	36.73	38.15	37.27
LR/HR	0.30	1.41	1.54	0.46	0.36	1.01	1.18	1.62	1.31	1.08	1.37	1.10	1.11	1.10	1.07	1.09	1.07
$(La/Yb)_N$	0.14	1.03	1.02	0.27	0.19	0.84	1.13	1.76	0.88	0.35	0.57	0.39	0.39	0.38	0.36	0.37	0.34
δEu	2.20	0.55	0.47	0.22	0.88	0.50	0.05	0.75	0.83	1.03	1.00	0.98	0.98	1.01	1.03	1.02	0.97
$(La/Sm)_N$	11.90	5.19	3.35	2.00	7.73	3.47	4.63	2.56	4.70	0.36	0.59	0.38	0.37	0.36	0.35	0.36	0.35
Y	0.44	0.60	0.73	0.45	0.77	0.51	0.34	0.42	0.68	27.1	30.2	25.6	26.5	26.3	25.5	26.9	26.0
Ni	2250	2123	2001	2442	2554	2265	2450	2484	2283	73.7	172	60.8	73.1	62.3	72.4	73.3	78.3
Cr	2977	3033	3110	1956	2798	2876	2232	2479	3157	106	170	90.9	116	91.7	100	95.9	103
V	54.75	63.60	64.60	45.56	69.72	58.06	34.21	34.09	70.24	334	335	328	333	329	322	336	323
Zr	0.12	0.22	0.75	0.12	0.14	0.07	0.12	0.13	0.24	39.1	57.8	36.6	38.5	36.9	34.7	35.6	35.5
Rb	0.05	0.20	0.25	0.07	0.06	0.02	0.08	0.08	0.23	0.80	0.46	0.60	0.56	0.60	0.30	0.51	0.50
Sr	0.49	0.51	1.89	0.58	0.59	0.46	0.49	0.74	0.64	134	24.0	125	122	134	112	102	124
Ba	0.97	2.15	2.34	0.91	1.34	0.84	0.94	1.32	1.92	5.47	5.38	9.19	4.14	5.73	8.81	11.1	8.20
Th	0.01	0.05	0.07	0.01	0.01	0.01	0.01	0.01	0.05	<0.05	0.06	0.10	<0.05	0.07	<0.05	<0.05	<0.05
U	0.02	0.06	0.02	0.01	0.02	0.14	0.15	0.68	0.13	<0.05	<0.05	<0.05	<0.05	<0.05	<0.05	<0.05	<0.05
Pb	<0.05	<0.05	<0.05	<0.05	<0.05	<0.05	<0.05	<0.05	<0.05	0.07	0.42	0.30	0.14	0.13	0.04	0.14	<0.05
Nb	0.01	0.03	0.09	0.01	0.01	0.01	0.01	0.02	0.03	1.06	1.06	1.10	1.01	1.01	0.98	1.04	1.02
Ta	0.01	0.01	0.01	0.01	0.01	0.01	0.01	0.01	0.01	0.08	0.08	0.09	0.08	0.09	0.08	0.08	0.09
Hf	0.00	0.01	0.02	0.01	0.01	0.00	0.00	0.01	0.01	1.41	1.92	1.27	1.48	1.34	1.23	1.33	1.32

peridotite region (Fig. 8). Fig. 8b shows that the residual degree of partial melting of the Dangqiong mantle peridotite is 15%–25%. In addition, the TiO_2 content of the Dangqiong mantle peridotite is very low (<0.1%) (Table 7), which is a typical feature of the Alps ophiolite (Lugovi et al., 1991; Parlak and Delaloye, 1999; Melcher et al., 2002).

The nine mantle peridotite samples have very low REE contents, and their ΣREE contents range from 0.39 ppm–1.31 ppm, their LREE/HREE values range from 0.30–1.62, their $(La/Yb)_N$ values range from 0.14–1.76, and their $(La/Sm)_N$ values range from 2–11.9. Although these REE contents vary slightly, their distribution patterns are very consistent. The mantle peridotite exhibits a "V"-type primitive mantle-normalized REE distribution pattern (McDonough and Sun, 1995) (Fig. 9a). All but two of the samples are enriched in LREE. Only one lherzolite sample has an enriched δEu value of 2.2; the other samples record depleted δEu values of 0.05–0.88.

The REE pattern of the Dangqiong mantle peridotite is distinctively different from the LREE-depleted pattern of the Alpine peridotite (Dymek et al., 1988), which is a "V"-type pattern, with low total REE contents that are highly depleted. Combined with its high MgO contents, it implies that the Dangqiong mantle peridotite has successively experienced high degrees of partial melting and fluid metasomatism during subduction (Qiu et al., 2005).

The contents of compatible elements in these samples,

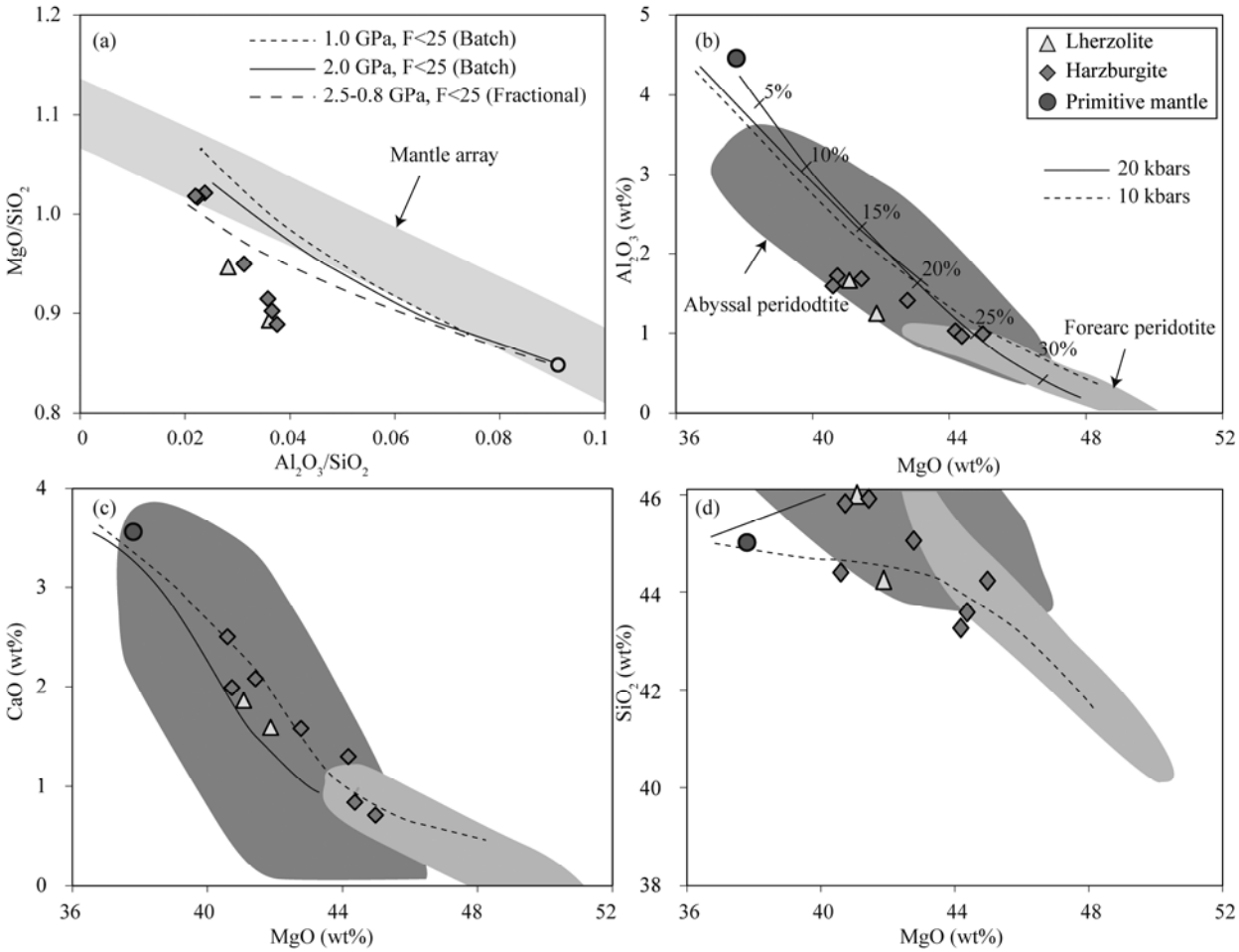

Fig. 8. Harker diagrams showing the whole-rock compositional ranges of the lherzolites and harzburgites of the Dangqiong ophiolite (primitive mantle values are from McDonough and Sun, 1995).
(a) Plot of Al_2O_3/SiO_2 vs. MgO/SiO_2, in which the mantle trend line is based on the model (Hart and Zindler, 1986; Jagoutz et al., 1979) and the mantle source region changes in pressure melting and crystallization evolution line (Marchesi et al., 2006; Niu et al., 1997); (b) Plot of MgO vs. Al_2O_3, Dangqiong peridotite are in the melt evolution trend line that based on the model of Niu et al.(1997), represented 15 to 25 percent partial melting; Abyssal and forearc peridotite fields are after Niu et al. (1997) and Parkinson and Pearce (1998), respectively. Also shown are residual compositions after from melting (at 10kb and 20kb) of the primitive mantle (Palme and O'Neil, 2004) calculated using the pMELTS program for a maximum 40% melting degree (Ghiorso et al., 2002). Clinopyroxene disappear after MgO=44 for 10 kb and MgO=42 for 20 kb (indicated by ticks on the melting curves); similar legend in the behind figure; (c) Plot of MgO vs. CaO; (d) Plot of MgO vs. SiO_2.

such as Cr and Ni, are generally as high as 1956 ppm–3157 ppm and 2001 ppm –2554 ppm (Table 7), respectively, indicating that these elements had not been affected by serpentinization. The low contents of LILE, such as Rb (0.02 ppm–0.25 ppm) (Table 7), are similar to the general features of typical ophiolites, indicating the characteristics of residual mantle rocks. According to Fig. 10, Y, V and Yb are negatively correlated with MgO, and Ni is positively correlated with MgO, implying that they exhibit a certain relation to the contents of spinel and olivine (Dick and Bullen, 1984). The Dangqiong mantle peridotite has higher Ni contents and lower Y, V and Yb contents than the primitive mantle (Fig. 10), which may be the result of the relative enrichment of compatible elements (such as Ni) and the depletion of incompatible elements (such as Al, Ca, Y, V and Yb) in the residual solid phase during the process of partial melting.

Similar to major elements, most of the trace elements in the Dangqiong mantle peridotite plot in the abyssal mantle peridotite region, with several samples plotted in the overlapping area between the abyssal and subduction types (Fig. 10).

The primitive mantle-normalized diagram of the mantle peridotite shows right dipping patterns (Fig. 9b). The enrichment of large ionic lithophile elements (LILE) resulted from crustal fluid of the subduction zone. In addition, high field strength elements exhibit both depletion of Nb, HREE and Th and enrichment of Ta, Ce and U, indicating the depleted mantle source and different degrees of fluid metasomatism in the subduction zone.

All of the lherzolites and harzburgites have similar primitive mantle-normalized trace element patterns that are strongly depleted in lithophile elements, with concentrations well below those of abyssal peridotites (Niu, 2004; Bodinier and Godard, 2007). The peridotites are characterized by very strong negative Sm anomalies

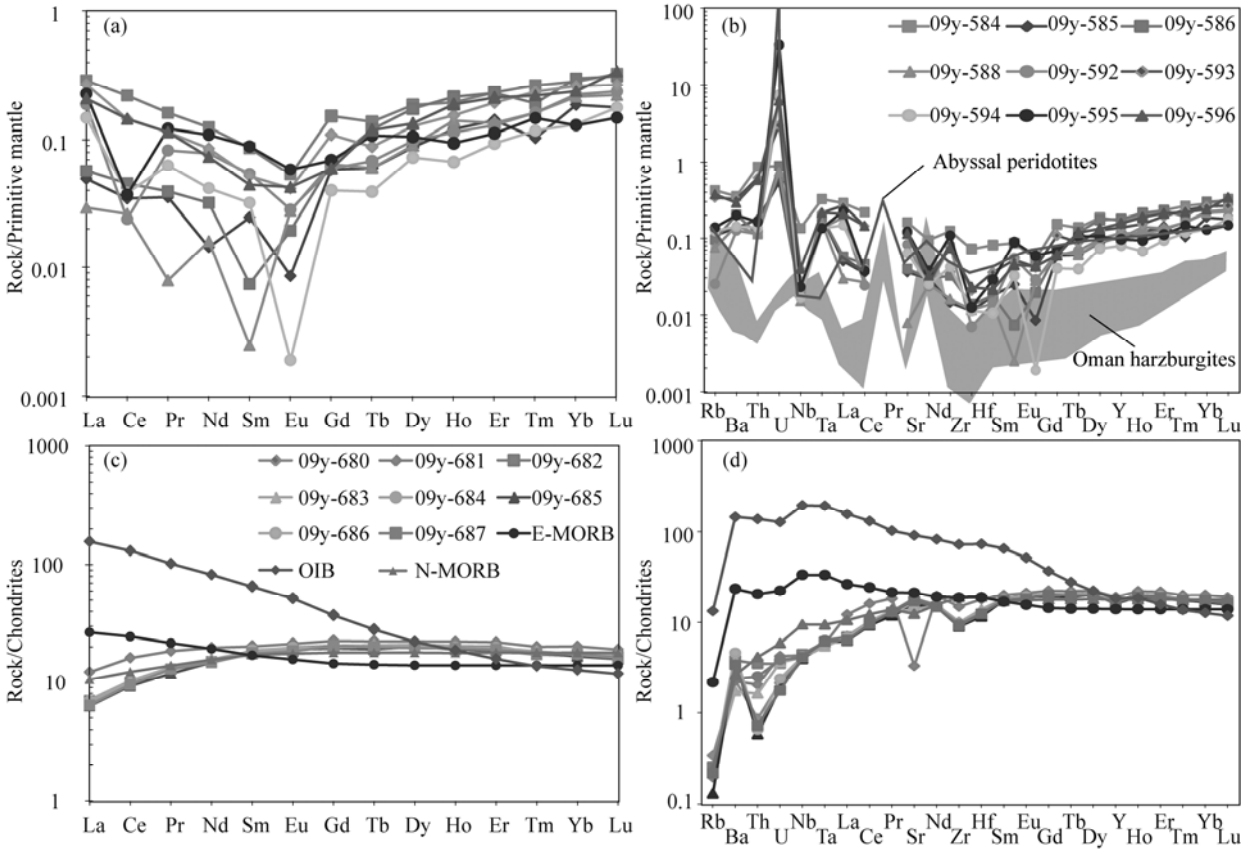

Fig. 9. REE pattern and spider diagram of the mantle peridotites and gabbro of the Dangqiong ophiolite.
(a) Primitive mantle-normalized REE patterns of the harzburgites and lherzolites (normalizing values are from McDonough and Sun, 1995); (b) primitive mantle-normalized trace element spider diagrams for the harzburgites and lherzolites (normalizing values are from McDonough and Sun, 1995); (c) chondrite-normalized REE patterns of gabbro (normalizing values are from Sun and McDonough, 1989); (d) chondrite-normalized trace element spider diagrams for gabbro (normalizing values are from Sun and McDonough, 1989).
The average composition of abyssal peridotites (red line) is from Niu (2004) and Bodinier and Godard (2007). The compositions of harzburgite sampled in the Semail (Oman) ophiolite are from Godard et al. (2000).

and positive U anomalies (Fig. 9b). Generally, the spider diagrams show that the Dangqiong peridotites are compositionally similar to the abyssal peridotites and harzburgites of the Oman ophiolite (Godard et al., 2000).

4.3.2 Gabbro

Whole-rock geochemical analyses were performed on 8 gabbro samples from the Dangqiong ophiolite. The average LOI value was 2.3%, indicating the weak alteration of these samples, similar to that observed under the microscope. These samples had variable Al_2O_3 and CaO contents ranging from 14.83–16.2 (wt%) and 11.77–15.5 (wt%), respectively. When normalized to the C1 chondritic values, the REE and trace element contents of these rocks showed an N-MORB-type pattern (Fig. 9c–d). These rocks were slightly depleted in highly incompatible (LREE) elements with respect to less incompatible elements (HREE), with La/Yb_N values ranging from 0.34 to 0.57 and weak negative Ta-Nb anomalies, suggesting the presence of a subduction component.

4.4 Discussion

4.4.1 Tectonic setting of the mafic dykes

Determining the tectonic setting of ophiolite formation is important for restoring the tectonic framework of a region in the geological history. Some elements, such as Hf, Ti, Zr, Y, Nb and Sr, are the most effective discriminant factors for distinguishing basalts from different tectonic environments (Pearce and Cann, 1971, 1973). On the Ta/Yb vs. Th/Yb diagram (Fig. 11a), the gabbro plots in the MORB area, and on the Hf/3-Th-Ta diagram (Fig. 11b), the gabbro plots in the N-MORB area. On the Nb/Yb vs. TiO_2/Yb graph of Pearce (2008), the Dangqiong gabbro plots close to the N-MORB field but have lower Nb/Yb ratios (Fig. 11c), indicating that the source of this gabbro was more depleted than the N-MORB source. On the discrimination diagram of Pearce and Norry (1979), the gabbro plots in the N-MORB and volcanic arc basalt fields (Fig. 11d).

Together, the above mentioned diagrams of inactive elements indicate that the Dangqiong gabbro is characterized as N-MORB, which formed in a mid-ocean ridge setting and was overlaid by the characteristics of oceanic island basalts. The discovery of amphibole in the Dangqiong gabbro suggests that alteration occurred later and was driven by fluids from a subducted plate (Ionov et al., 1997; Coltorti et al., 2004).

The Luobusa and Purang ophiolites in the eastern and

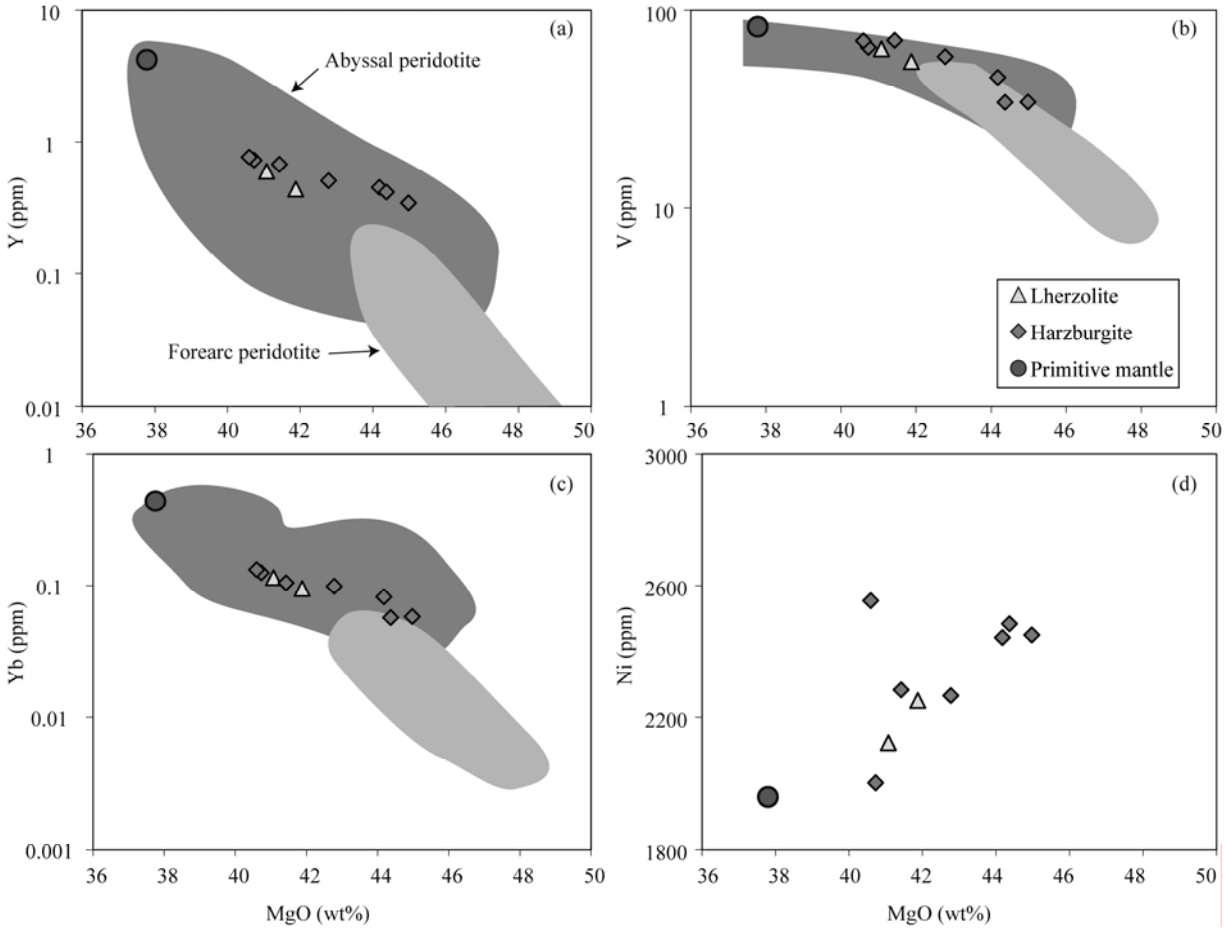

Fig. 10. MgO variation diagram of the trace element contents of the lherzolites and harzburgites of the Dangqiong ophiolite (primitive mantle values are from McDonough and Sun, 1995).
(a) Plot of MgO vs. Y, Abyssal and forearc peridotite fields are after Niu et al. (1997) and Parkinson and Pearce (1998), respectively; (b) Plot of MgO vs. V; (c) Plot of MgO vs. Yb; (d), Plot of MgO vs. Ni

western segments of the Yarlung-Zangbo Suture Zone both experienced a SSZ evolution after having formed in a mid-ocean ridge setting (Liu et al., 2010; Xu et al., 2011a, 2011b; Li et al., 2015). The ophiolite in the Dangqiong area discussed here may also belong to this type.

4.4.2 Petrogenesis of the Dangqiong peridotites

Harzburgite and lherzolite in Dangqiong have high MgO contents and low Al_2O_3, CaO and TiO_2 contents; they thus represent the medium to strongly depleted residual mantle, which represents the residual depleted mantle remaining after remelting. The petrological and geochemical analysis shows that the Dangqiong mantle peridotite exhibit the features of both abyssal and subduction mantle peridotites.

The chemical compositions of the main minerals from the ultramafic and mafic rocks reflect the different affinities and petrogenesis of the Dangqiong ophiolitic massif. The olivine from the Dangqiong peridotite is from forearc and upper mantle abyssal peridotites (Fig. 4). According to the $Mg^{\#}$ and $Cr^{\#}$ values of spinel (Fig. 6), the Dangqiong peridotites plot within the field of abyssal peridotite. In addition, when the $Cr^{\#}$ values of spinel are plotted against the $Mg^{\#}$ values of olivine (Fig. 12), the Dangqiong peridotites exhibit a deeper mantle provenance (>20 kbar). The compositions of the Dangqiong peridotites resemble the compositions of abyssal peridotites. Compared to the orthopyroxenes from modern settings, the orthopyroxenes in the peridotites are compositionally similar to those of abyssal peridotites (Fig. 5b). The compositions of the clinopyroxenes in the peridotites from Dangqiong are similar to the compositions of the clinopyroxenes from modern abyssal peridotites (Fig. 5d). The compositional range of the clinopyroxene from the gabbro has low Cr_2O_3 contents that fall within those of back-arc-basin basalts (BABB) (Fig. 5d). Thus, the mantle rocks from the Dangqiong ophiolitic massif appear to be comparable to abyssal peridotites. The mineral chemistry data show that the Dangqiong mafic was formed in a back-arc environment.

4.4.3 Tectonic setting of the Dangqiong ophiolite

Ophiolites represent the remnants of ancient oceanic lithosphere in continental orogenic belts; they record the magmatic evolution, metamorphism and tectonic processes of the oceanic lithosphere and provide important information about the formation, development and extinction of ancient ocean basins and thus have always

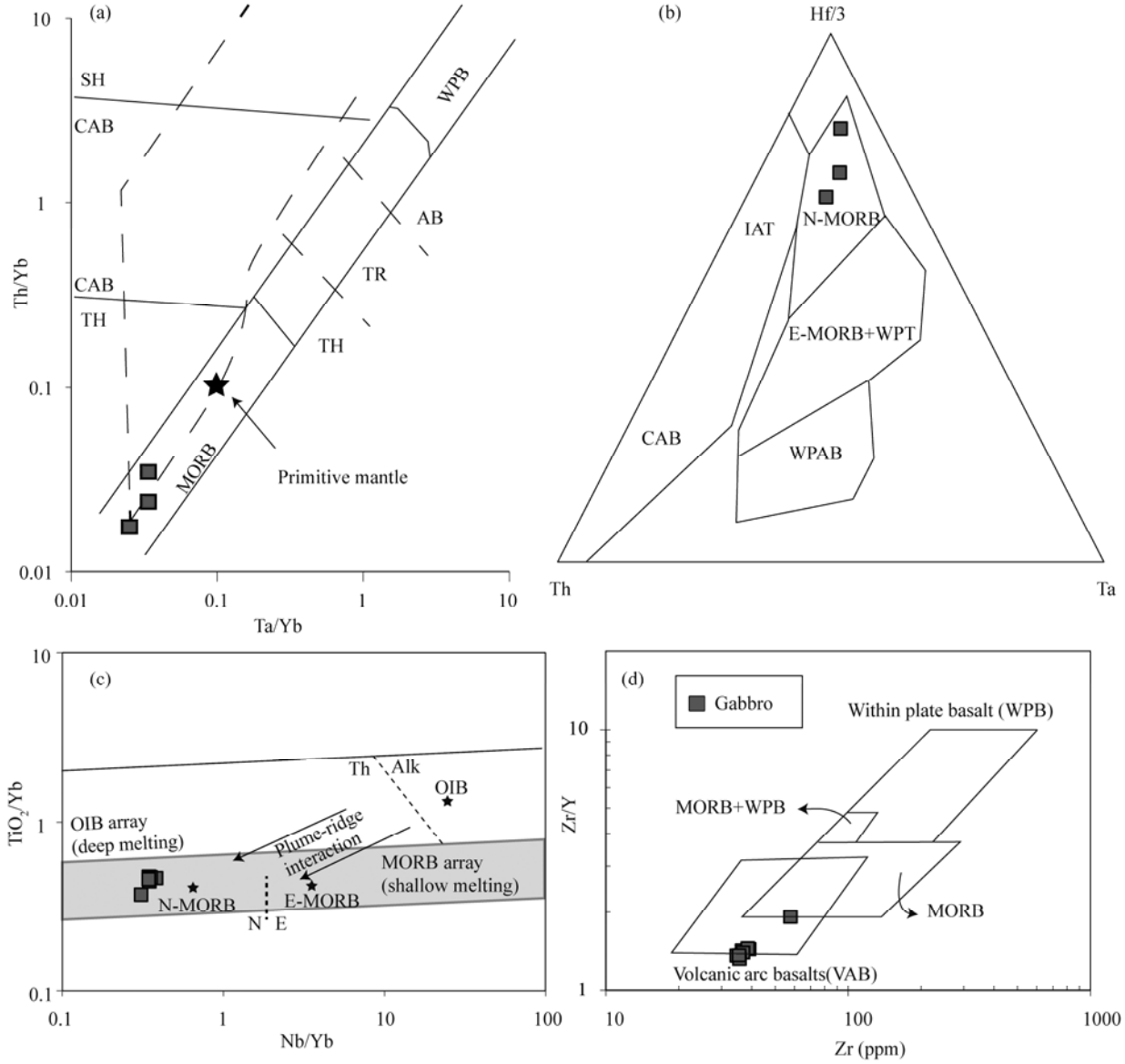

Fig. 11. Tectonic environment discrimination diagram for gabbros from the Dangqiong ophiolite.
(a) diagram of Ta/Yb vs. Th/Yb (Pearce, 1984); (b) diagram of Th vs. Ta vs Hf/3 (Wood, 1980); (c) diagram Nb/Yb vs. TiO_2/Yb, the grey field outlines the MORB-OIB array (Pearce, 2008). OIB, N-MORB and E-MORB are from Sun and McDonough (1989). Th = tholeiitic OIB, Alk = alkalic OIB. Arrows show the plume-ridge interaction trend; (d) diagram of Zr vs. Zr/Y (Pearce et al., 1979), MORB= mid-ocean ridge basalt, WPB= intraplate basalts, CAB= calc-alkali basalt, SH= mugearite, TH= tholeiite, TR= transition basalt, IAT= island-arc tholeiites.

been a focus of geoscientific research. Ophiolites are divided into two types based on the tectonic environment of their formation: MOR (mid-ocean ridge) and SSZ (supra subduction zone) ophiolites (Pearce et al., 1984). Recently, the other two types, including those related and not related to subduction based on their different geochemical and tectonic characteristics, have also been identified (Dilek et al., 2011).

The ophiolite in the Yarlung-Zangbo Suture Zone, Tibet, has long been studied due to its relatively new formation and good preservation. Various dynamic models have been proposed to explain the formation mechanism of the Yarlung-Zangbo Suture Zone: (1) the remnants of oceanic crust fragments from the mid-ocean ridge of the new Tethys Ocean (Nicolas et al., 1981; Girardeau et al., 1985a, b); (2) oceanic crust that formed in an island arc and continental margin (Wang, 1987; Pan et al., 1997); (3) the formation and evolution of the Yarlung-Zangbo Suture Zone in a supra subduction zone (SSZ) tectonic environment (Pearce et al., 1984; Wang et al., 2000; Hébert et al., 2012); (4) formation in a MOR environment followed by varying degrees of alteration in a SSZ environment (Yang et al., 2011; Xiong et al., 2011, 2016b; Xu et al., 2011a, 2011b; Li et al., 2015; Feng et al., 2017; Lai et al., 2018). These models have indicated the different factors the affect the formation processes of ophiolite.

In recent years, due to the improved traffic conditions in this area and the implementation of a chromitite resource investigation project in China, various studies have been performed on the petrology, mineralogy, geochemistry and

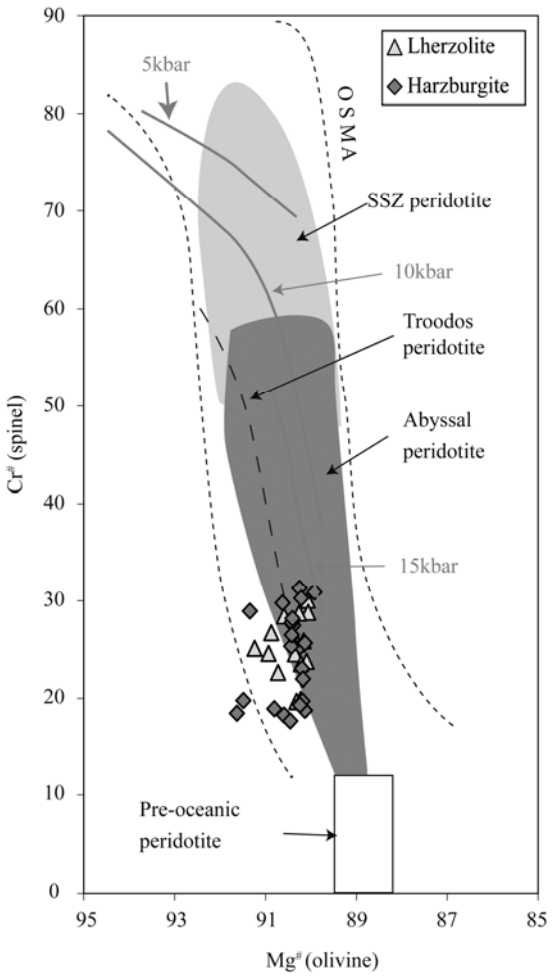

Fig. 12. Polybaric origin of the Dangqiong ophiolitic massif peridotites deduced based on the $Cr^{\#}$ values in spinels and coexisting $Mg^{\#}$ values in olivines.

The olivine-spinel mantle array (OSMA; dotted field) and compositional range in abyssal peridotites are from Arai (1994). The compositional ranges in pre-oceanic peridotites are from Bonatti and Michael (1989) and in supra-subduction zone (SSZ) peridotites are estimated from published data by Pearce et al. (2000). The dashed line represents themean compositional variations in the Troodos peridotites (Sobolev and Batanova, 1995). The 5 and 10 kbar curves are from Sobolev and Batanova (1995), and the 15 kbar curve is from Jaques and Green (1980).

chronology of these ophiolites (Huang et al., 2006; Xu et al., 2006; Wei et al., 2006; Liu et al., 2010). The geochemical characteristics of these mafic rocks indicate that the Daba-Xiugugabu ophiolite has preserved the features of both MORB and SSZ (Xu, 2006; Bezard et al., 2011). The analysis of the Purang ophiolite in the western segment of the belt also shows that the two tectonic environments of MORB and SSZ formed in the collision zone after the ancient ocean disappeared, i.e., reflecting the formation of an early MORB and later SSZ environment (Xu et al., 2008; Liu et al., 2010; Xu et al., 2011a; Li et al., 2015).

Since beginning of the Late Triassic, the northern margin of the generally northward-moving Himalaya plate started to disintegrate due to the plume activity of the upper mantle, i.e., the strata split from the northern margin of the Himalaya plate, and a small ocean basin formed in the middle. The marginal ocean basin corresponds to the location where the Dangqiong ophiolite formed (Xia et al., 1998). There are several similarities and differences between the Dangqiong ophiolites and other YZSZ ophiolites (see Hébert et al., 2003; Dubois-Côté et al., 2005). The development of the Dangqiong ophiolite in the western segment may have occurred earlier than that of the Xigaze ophiolite in the middle segment and the Luobusa and Zedang ophiolites in the eastern segment. The Sm-Nd internal isochron age of the four mafic Xiugugabu dykes is 126.2±9.1 Ma, and the zircon SHRIMP U-Pb age of the Xiugugabu diabase is 122.3±2.4 Ma, which is considered the formation age of the Daba-Xiugugabu Tethys ocean basin and is similar to the formation age in the middle section (126±1.5 Ma) (Wei et al., 2006; Xu et al., 2007).

MgO content of the Dangqiong mantle peridotite is dramatically higher than that of the primitive mantle. The REE distribution diagram shows a "V"-type pattern. The trace element contents of the Dangqiong peridotites suggest that these rocks were generated in a zone where magmatic fluids or melts interacted with mantle rocks. The mineral chemical compositions of the ultramafic rocks in the Yarlung-Zangbo ophiolites reflect intermediate compositions between abyssal and forearc peridotites (Bédard et al., 2009; Hébert et al., 2003). The amphibole compositions of the mafic intrusions fallt in the field of amphibole from an ophiolitic mélange (Fig. 7) (Dupuis et al., 2005). The whole-rock geochemical compositions indicate N-MORB-type patterns for REEs and trace elements (Fig. 9c–d). These patterns are slightly depleted in highly incompatible elements (LREE) with respect to less incompatible elements (HREE), with weak negative Ta-Nb anomalies, suggesting the presence of a subduction component. These features imply a depleted mantle source, which later recorded fluid alteration in a subduction zone. In conclusion, the Dangqiong ophiolite formed in a MOR setting and was modified by fluids in a SSZ setting, similar to the Luobusa ophiolite in the eastern Yarlung-Zangbo Suture Zone and the Purang ophiolite in the western Yarlung-Zangbo Suture Zone.

5 Conclusion

(1) The Dangqiong ophiolitic massif consists mainly of harzburgite, with minor dunite and lherzolite, suggesting the involvement of mantle material. Based on field investigation, the results in this study indicate that these peridotites may source from deeper mantle (>20 kbar). The composition of the Dangqiong peridotites is similar to that of abyssal peridotites.

(2) The Dangqiong gabbros show N-MORB-type patterns of REEs and trace elements. These patterns are slightly depleted in highly incompatible elements (LREE) with respect to less incompatible elements (HREE), with $[La/Yb]_{CN}$ values ranging from 0.34 to 0.57 and weak negative Ta-Nb anomalies, suggesting the presence of a subduction component. Combined with the diagram of the above inactive elements, it indicates that the Dangqiong gabbro is characterized as N-MORB and late recorded the characteristics of oceanic island basalts. The presence of

amphibole in the Dangqiong gabbro suggests the late-stage alteration of subduction-derived fluids.

(3) All of the lherzolites and harzburgites in Dangqiong have similar distribution patterns of REEs and trace elements, with relatively concentrated LREE contents, distinct Eu anomalies, depleted high field strength element contents (such as Nb, HREE and Th) and relatively enriched Ta, Ce and U contents, implying a depleted mantle source and fluid alteration in the subduction zone. These features suggest that the Dangqiong ophiolite formed in two different structural settings (MORB and SSZ), which is inconsistent with the formation setting of the Luobusa ophiolite in the eastern Yarlung-Zangbo Suture Zone and the Purang ophiolite in the western Yarlung-Zangbo Suture Zone. These data imply that the ophiolites in this suture zone are characteristic of the two-stage evolution.

Acknowledgments

We thank two anonymous reviewers for their constructive and thorough reviews that helped us improve the paper. This research was funded by grants from the NSF China (No. 41672046, 41720104009), the China Geological Survey (DD20160023-01), the Ministry of Science and Technology (201511022) and IGCP (International Geoscience Programme) Project 649.

Manuscript received Aug. 1, 2018
accepted Dec. 20, 2018
associate EIC YANG Jingsui
edited by FEI Hongcai

References

Arai, S., 1994. Characterization of spinel peridotites by olivine-spinel compositional relationships: review and interpretation. *Chemical Geology*, 113: 191–204.

Bédard, É., Hébert, R., Guilmette, C., Lesage, G., Wang, C.S., and Dostal, J., 2009. Petrology and geochemistry of the Saga and Sangsang ophiolitic massifs, Yarlung Zangbo Suture Zone, Southern Tibet: Evidence for an arc-back-arc origin. *Lithos*, 113: 48–67.

Bezard, R., Hébert, R., Wang, C.S., Dostal, J., Dai, J.G., and Zhong, H.T., 2011. Petrology and geochemistry of the Xiugugabu ophiolitic massif, western Yarlung Zangbo suture zone, Tibet. *Lithos*, 125: 347–367

Bodinier, J.L., and Godard, M., 2007. Orogenic, ophiolitic, and abyssal peridotites. *Treatise on Geochemistry*, 2: 1–73.

Bonatti, E., and Michael, P.J., 1989. Mantle peridotites from continental rifts to ocean basins to subduction zones. *Earth and Planetary Science Letters*, 91: 297–311.

Coleman, R.G., 1977. *Ophiolites, Ancient Oceanic Lithosphere*. Belin: Springer-Verlag, 2–10.

Coltorti, M., Beccaluva, L., Bonadiman, C., Faccin, B., Ntaflos, T., and Siena, F., 2004. Amphibole genesis via metasomatic reaction with clinopyroxene in mantle xenoliths from Victoria Land, Antarctica. *Lithos*, 75(1–2): 115–139.

Coltorti, M., Bonadiman, C., Faccini, B., Grégoire, M., O'Reilly, S.Y., and Powel, W., 2007. Amphiboles from suprasubduction and intraplate lithospheric mantle. *Lithos*, 99(1–2): 68–84.

Constantin, M., 1999. Gabbroic intrusions and magmatic metasomatism in harzburgites from the Garrett transform fault: implications for the nature of the mantle–crust transition at fast-spreading ridges. *Contributions to Mineralogy and Petrology*, 136: 111–130.

Constantin, M., Hékinian, R., Ackermand, D., and Stoffers, P., 1995. Mafic and ultramafic intrusions into upper mantle peridotites from fast spreading centers of the Easter microplate (South East Pacific). In: Vissers, R.L.M., and Nicolas, A. (eds.), *Mantle and Lower Crust Exposed in Oceanic Ridges and in Ophiolites.* Kluwer, Dordrecht, Netherlands, 71–120.

Dick, H.J.B., and Bullen, T., 1984. Chromian spinel as a petrogenetic indicator in abyssal and alpine-type peridotites and spatially associated lavas. *Contributions to Mineralogy and Petrology*, 86: 54–76.

Dick, H.J.B, and Natland, J.H., 1996. Late stage melt evolution and transport in the shallow mantle beneath the East Pacific Rise. In: Mevel, C., Gillis, K.M., Allan, J.F. and Meyer, P.S. (eds.), *Proceedings of the Ocean Drilling Program.* Scientific Results, 147: 103–134.

Dick, H.J.B., 1977. Partial melting in the Josephine Peridotite-1, the effect of mineral composition and its consequence from geobarometry and geothermometry. *American Journal of Science*, 227: 801–832.

Dilek, Y., and Furnes, H., 2011. Ophiolite genesis and global tectonics: Geochemical and tectonic fingerprinting of ancient oceanic lithosphere. *Geological Society of America Bulletin*, 123(3–4): 387–411.

Dubois-Côté, V., Hébert, R., Dupuis, C., Wang, C.S., Li, Y.L., and Dostal, J., 2005. Petrological and geochemical evidence for the origin of the Yarlung Zangbo ophiolites, southern Tibet. *Chemical Geology*, 214: 265–286.

Dupuis, C.V., Hèbert, R., Dubois-Côtè, V., Guilmette, C., Wang, C.S., Li, Y.L., and Li, Z.J., 2005. The Yarlung Zangbo Suture zone ophiolitic melange (Southern Tibet): new insights from geochemistry of ultramafic rocks. *Journal of Asian Earth Sciences*, 25: 937–960.

Dymek, R.F., Brothers, S.C., and Schiffries, C.M., 1988. Petrogenesis of ultramafic metamorphic rocks from the 3800 Ma Isua Supracrustal Belt, west Greeland. *Journal of Petrology*, 29: 1353–1397.

Feng, G.Y., Yang, J.S., Yildirim, D., Liu, F., and Xiong, F.H., 2017. Petrological and Re-Os Isotopic Constraints on the Origin and Tectonic Setting of the Cuobuzha Peridotite, Yarlung Zangbo Suture Zone, SW Tibet, China. *Acta Geologica Sinica* (English Edition), 91(supp.1): 10–11.

Feng, G.Y., Yang, J.S., Xiong, F.H., Liu, F., Niu, X.L., Lian, D.Y., Wang, Y.P., Zhao, Y.J., 2015, Petrology, geochemistry and genesis of the Cuobuzha peridotite in the western Yarlung Zangbo suture zone. *Geology in China*, 42 (5): 1337−1353 (in Chinese with English abstract).

Frey, F.A., Suen, C.J., and Stockman, H.W., 1985. The Ronda high temperature peridotite: geochemistry and petrogenesis. *Geochimica et Cosmochimica Acta*, 49: 2469–2491.

Gansser, A., 1983. Suture zone of Indian- circling. Institute of Geology, Chinese Academy of Geological Sciences (ed.). Geology of Tethys Structural Belt. *Beijing: Geological Publishing House*, 58–67 (in Chinese).

Ghiorso, M.S., Hirschmann, M.M., Reiners, P.W., and Kress, III.V.C., 2002. The pMELTS: A revision of MELTS for improved calculation of phase relations and major element partitioning related to partial melting of the mantle to 3 GPa. *Geochemistry, Geophy*sics, *Geosystems,* 3(5): 1–35.

Girardeau, J., Mercier, J.C.C., and Wang, X., 1985a. Petrology of the mafic rocks of the Xigaze ophiolites, Tibet: implications for the genesis of the oceanic lithosphere. *Contributions to Mineralogy and Petrology*, 90: 309–321.

Girardeau, J., Mercier, J.C.C., and Zao, Y., 1985b. Structure of the Xigaze ophiolite, Yarlung Zangbo suture zone, southern Tibet, China: genetic implications. *Tectonics*, 4: 267–288.

Godard, M., Jousselin, D., and Bodinier, J.L., 2000. Relationships between geochemistry and structure beneath a palaeo-spreading Centre: a study of the mantle section in the Oman Ophiolite. *Earth & Planetary Science Letters*, 180: 133 –148.

Guo, T.Y., Liang, D.Y., Zhang, Y.Z., and Zhao, C.H., 1991. *Geology of Ngari, Tibet* (Xizang). Wuhan: The China University of Geosciences Press, 464 (in Chinese with English abstract).

Hart, S.R., and Zindler, A., 1986. In search of a bulk-Earth composition. *Chemical Geology*, 57(3–4): 247–267.

Hartmann, G., and Wedepohl, K.H., 1993. The composition of peridotite tectonics from the Ivrea complex, northem Italy, residues from melt extraction. *Geochemica et Cosmochemica Acta*, 57:1761 – 1782.

Hawkins, J.W., and Allan, J.F., 1994. Petrologic evolution of Lau Basin sites 834 through 839. *Texas: Proceedings of the Ocean Drilling Program: Scientific Results*, 135, 427–470.

Hébert, R., Bezard, R., and Guilmette, C., 2012. The Indus-Yarlung Zangbo ophiolites from Nanga Parbat to Namche Barwa syntaxes, southern Tibet: first synthesis of petrology, geochemistry, and geochronology with incidences on geodynamic reconstructions of Neo-Tethys. *Gondwana Research*, 22(2): 377–397.

Hébert, R., Huot, F.,Wang, C.S., and Liu, Z., 2003. Yarlung Zangbo ophiolites, southern Tibet revisited: geodynamic implications from the mineral record. In: Dilek, Y., and Robinson, P.T. (eds.), *Ophiolites in Earth History*, Geological Society of London Special Publication, 218:165–190.

Hirose, K., and Kawamoto, T., 1995. Hydrous partial melting of lherzolite at 1 GPa: the effect of H_2O on the genesis of basaltic magmas. *Earth and Planetary Science Letters*, 133: 463–473.

Huang, G.C., Mo, X.X., Xu, D.M., Lei, Y.J., and Li, L.J., 2006. Origination and evolution of Daba-Xiugugabu ophiolite belt in the Southwestern Tibet. *Geology and Mineral Resources of South China*, 3: 1–9 (in Chinese with English abstract).

Huot, F., Hébert, R., Varfalvy, V., Beaudoin, G., Wang, C., Liu, Z., Cotten, J., and Dostal, J., 2002. The Beimarang Melange (southern Tibet) brings additional constraints in assessing the origin, metamorphic evolution and obduction processes of the Yarlung Zangbo ophiolite. *Journal of Asian Earth Sciences*, 21: 307–322.

Ionov, D.A., GriffinN, L.W., and O'Reilly, S.Y., 1997. Volatile-bearing minerals and lithophile trace elements in the upper mantle. *Chemical Geology*, 141: 153–184.

Ishii, T., Robinson, P.T., Maekawa, H., and Fiske, R., 1992. Petrological studies from diapiric serpentine seamounts in the Izu-Ogazawara-Mariana forearc, Leg125. In: Fryer, P., Pearce, J.A., and Stokking, L.B. (eds.), P*roceedings of the Ocean Drilling Program, Scientific Results*, 125: 445–486.

Jagoutz, E., Palme, H., Baddenhausen, H., Blum, H., Cendales, M., Dreibus, G., Spettel, B., Lorenz, V., and Wanke, H., 1979. The abundance of major, minor and trace elements in the Earth's mantle as derived from primitive ultramafic nodules. *Geochimica Et Cosmochimica Acta*, 10: 2031–2050.

Jaques, A.L., and Green, D.H., 1980. Anhydrous melting of peridotites at 0-15 kbar pressure and the genesis of tholeiitic basalts. *Contributions to Mineralogy and Petrology*, 73: 287–310.

Jiang, M., Yang, J.S., Zhang, L.S., Zhang, Y.W., Peng, M., and Li, Q.Q., 2016. The magnetic anomaly characteristics of Dongpo, Xigaze and some other ophiolite rock masses along the Yarlung-Zangbo suture zone and their oreprospecting significance. *Geology in China*, 43(5): 1666–1678 (in Chinese with English abstract).

Johnson, K.T.M., Dick, H.J.B., and Shimizu, N., 1990. Melting in the oceanic uppermantle: an ion microprobe study of diopsides in abyssal peridotites. *Journal of Geophysical Research*, 95: 2661–2678.

Lai, S.M., Yang, J.S., Yildirim, D., Xiong, F.H., Jiang, R., and Chen, Y.H., 2018. Petrological and Os Isotopic Characteristics of Zedong Peridotites in the Eastern Yarlung–Zangbo Suture in Tibet. *Acta Geologica Sinica* (English Edition), 92(2): 442–461

Leake, B.E., Wooley, A.R., Arps, C.E.S., Birch, W.D., Gilbert, M.C., Grice, J.D., Hawthorne, F.C., Kato, A., Kisch, H.J., Krivovichev, V.G., Linthout, K., Laird, J., Mandarino, J.A., Maresch, W.V., Nickel, E.H., Rock, N.M.S., Schumacher, J.C., Smith, D.C., Stephenson, N.C.N., Ungaretti, L., Whittaker, E.J.W., and Guo Y.Z., 1997. Nomenclature of amphiboles: report of the subcommittee on amphiboles of the International Mineralogical Association Commission on new minerals and mineral names. *The Canadian Mineralogist*, 35: 219–246.

Leake, B.E., Woolley, A.R., Birch, W.D., Burke, E.A.J., Ferraris, G., Grice, J.D., Hawthorne, F.C., Kisch, H.J., Krivovichev, V.G., Schumacher, J.C., Stephenson, N.C.N., and Whittaker, E.J.W., 2004. Nomenclature of amphiboles; additions and revisions to the International Mineralogical Association's amphibole nomenclature. *American Mineralogist*, 89: 883–887.

Leblanc, M., 1980. Chromite growth, dissolution and deformation from a morphological view point: SEM investigations. *Mineralium Deposita*, 15(2): 201–210.

Li, X.P., Chen, H.K., Wang, Z.L., Wang, L.J., Yang, J.S., and Robinson, P., 2015. Textural evolution of spinel peridotite and olivine websterite in the Purang ophiolite complex, western Tibet. *Journal of Asian Earth Sciences*, 110: 55–71.

Liu, C.Z., Wu, F.Y., Wilde, S.A., Yu, L.J., and Li, J.L., 2010. Anorthitic plagioclase and pargasitic amphibole in mantle peridotites from the Yungbwa ophiolite (southwestern Tibetan Plateau) formed by hydrous melt metasomatism. *Lithos*, 114: 413–422.

Lugović, B., Altherr, R., Raczek, I., Hofmann, A.W., and Majer, V., 1991. Geochemistry of peridotites and mafic igneous rocks from the Central Dinaric Ophiolite Belt, Yugoslavia. *Contributions to Mineralogy and Petrology*, 106(2):201–216.

Luo, Z.H., 2019. The emplacement of the Yarlung Zangboo phiolites: A new analytical model. *Geology in China*, 46(1): 21–31 (in Chinese with English abstract).

Marchesi, C., Garrido, C.J., Godard, M., Proenza, J.A., Gervilla, F., and Blanco-Moreno, J., 2006. Petrogenesis of highly depleted peridotites and gabbroic rocks from the Mayari-Baracoa ophiolitic belt (Eastern Cuba). *Contributions to Mineralogy and Petrology*, 151(6): 717–736.

McDonough, W.F., and Sun, S.S., 1995. The composition of the Earth. *Chemical Geology*, 120 (3): 223–254.

Melcher, F., Meisel, T., Puhl, J., and Koller, F., 2002. Petrogenesis and geotectonic setting of ultramafic rocks in the Eastern Alps: Constraints from geochemistry. *Lithos*, 65(1): 69–112.

Miller, C., Thöni, M., Frank, W., Schuster, R., Melcher, F., Meisel, T., and Zanetti, A., 2003. Geochemistry and tectonomagmatic affinity of the Yungbwa ophiolite, SW Tibet. *Lithos*, 66: 155–172.

Morimoto, N., 1988. Nomenclature of pyroxene. *Acta Mineralogica*, 8(4): 289–305.

Nicolas, A., and Prinzhofer, A., 1983. Cumulative or residual origin for the transition zone in ophiolites: Structure evidence. *Journal of Petrology*, 24(2): 188–206.

Nicolas, A., Girardeau, J., Marcoux, J., Duprè, B., Wang, X.B., Cao, Y.G., Zeng, H.X., and Xiao, X.C., 1981. The Xigaze ophiolite (Tibet): a peculiar oceanic lithosphere. *Nature*, 294: 414–417.

Niu, Y.L., Langmuir, C.H., and Kinzler, R.J., 1997. The origin of abyssal peridotites: A new perspective. *Earth and Planetary Science Letters*, 152(1–4): 251–265.

Niu, Y., 2004. Bulk-rock major and trace element compositions of abyssal peridotites: implications for mantle melting, melt extraction and post-melting processes beneath mid-ocean ridges. *Journal of Petrology*, 45: 2423–2458.

Palme, H., and O'Neill, H.S.C., 2004. Cosmochemical estimates of mantle composition. In: Holland, H.D., and Turrekian, K.K. (eds.), *Treatise on Geochemistry*, 2: 1–38.

Pan, G.T., Chen, Z.L., Li, X.Z., Yan, A.J., Xu, X.S., Xu, Q., Jiang, X.S., Wu, Y.L., Luo, J.N., Zhu, T.X., and Peng, Y.M., 1997. *The Formation and Evolution of the East Tethyan*. Beijing: Geological Publishing Housem, 1–218 (in Chinese with English abstract).

Parkinson, I.J., and Pearce, J.A., 1998. Peridotites from the Izu–Bonin–Mariana forearc (ODP Leg 125), evidence for mantle melting, melt–mantle interaction in a suprasubduction zone setting. *Journal of Petrology*, 39: 1577–1618.

Parlak, O., and Delaloye, M., 1999. Precise $^{40}Ar/^{39}Ar$ ages from the metamorphic sole of the Mersin ophiolite (southern Turkey). *Tectonophysics*, 301(1): 145–158.

Pearce, J.A., and Cann, J.R., 1971. Ophiolite origin investigated by discriminant analysis using Ti, Zr and Y. *Earth and Planetary Science Letters*, 12: 339–349.

Pearce, J.A., and Cann, J.R., 1973. Tectonic setting of basic

volcanic rocks determined using trace element analyses. *Earth and Planetary Science Letters*, 19: 290–300.
Pearce, J.A., Lippard, S.J., and Roberts, S., 1984. Characteristics and tectonic significance of supra-subduction zone ophiolites. In: Kokelaar, B.P., and Howells, M.F. (eds.), *Marginal basin geology*. London: Geological Society of London Special Publication, Blackwell Scientific Publications, 16(1): 77–94.
Pearce, J.A., Barker, P.F., Edwards, S.J., Parkinson, I.J., and Leat, P.T., 2000. Geochemistry and tectonic significance of peridotites from the South Sandwich arc-basin system, South Atlantic. *Contributions to Mineralogy and Petrology*, 139: 36 –53.
Pearce, J.A., 2008. Geochemical fingerprinting of oceanic basalts with applications to ophiolite classification and the search for Archean oceanic crust. *Lithos*, 100:14–48.
Pearce, J.A., and Norry, M.J., 1979. Petrogenetic implications of Ti, Zr, Y, and Nb variations in volcanic rocks. *Contributions to Mineralogy and Petrology*, 69: 33–47.
Qiu, R.Z., Deng, J.F., Zhou, S., Li, T.D., Xiao, Q.H., Guo, T.Y., Cai, Z.Y., Li, G.L., Huang, G.C., and Meng, X.J., 2005. Ophiolite types in western Qinghai-Tibetan plateau-Evidences from petrology and geochemistry. *Earth Science Frontiers*, 12 (2):277–291 (in Chinese with English abstract).
Searle, M.P., Windley, B.F., Coward, M.P., Cooper, D.J.W., Rex, A.J., Rex, D., Li, T.D., Xiao, X.C., and Jan, M.Q., 1987. The closing of the Tethys and the tectonics of the Himalayas. *Geological Society of America Bulletin*, 98(6): 678–701.
She, Y., Zhu, X.K., He, Y., Ma, J.X., and Sun, J., 2017. The new discovery of the podiform chromitite in the Xigaze ophioLite, Yarlung Zangbo suture zone, Tibet. *Geology in China*, 44(3): 610–611 (in Chinese with English abstract).
Sobolev, A.V., and Batanova, V.G., 1995. Mantle lherzolites of the Troodos ophiolite complex, Cyprus: clinopyroxene geochemistry. *Petrology*, 3: 440–448.
Sun, S.S., and McDonough, W.F., 1989. Chemical and isotopic systematics of oceanic basalts: implications for mantle compositions and processes. In: Saunders, A.D., and Norry, M.J. (eds.), *Magmatism in the Ocean Basins*. London: Geological Society London Special Publications, 42:313–345.
Van der Laan, S.R., Arculus, R.J., Pearce, J.A., and Murton, B.J., 1992. Petrography, mineral chemistry, and phase relations of the basement boninite series of Site 786, Izu-Bonin forearc. In: Fryer, P., Pearce, J.A., and Stokking, L.B. (eds.), *Proceedings of the Ocean Drilling Program, Scientific Results*, 125: 171–201.
Wang, C.S., Liu, Z., and Hébert, R., 2000. The Yarlung Zangbo paleo-ophiolite, southern Tibet: implications for the dynamic evolution of the Yarlung Zangbo Suture Zone. *Journal of Asian Earth Sciences*, 18: 651–661.
Wang, X.B., Bao, P.S., and Deng, W.M., 1987. *Tibet ophiolite*. Beijing: Geological Publishing House (in Chinese).
Wei, Z.Q., Xia, B., Zhang, Y.Q., Wang, R., Yang, Z.Q., and Wei, D.L., 2006. SHRIMP zircon dating of diabase in the Xiugugabu ophiolite in Tibet and its geological implications. *Geotectonica et Metallogenia*, 30: 93–97 (in Chinese with English abstract).
Wood, D.A., 1980. The applications of a Th-Hf-Ta diagram to problems of tectonomagmatic classification and to establishing the nature of crustal contamination of basaltic lavas of the British Tertiary volcanic province. *Earth and Planetary Science Letters*, 50: 11–30.
Xia, B., Guo, L.Z., and Shi, Y.S., 1998. *The ophiolites and tectonostratigraphic terranes in Southwest Xizang (Tibet)*. Guangzhou: Zhongshan University Press, 1–83 (in Chinese with English abstract).
Xiong, F.H., Yang, J.S., Liang, F.H., Ba, D.Z., Zhang, J., Xu, X.Z., Li, Y., and Liu, Z., 2011. Zircon U-Pb ages of the Dongbo ophiolite in the western Yarlung Zangbo suture zone and their geological signification. *Acta Petrologica Sinica*, 27 (11): 3223–3238 (in Chinese with English abstract).
Xiong, F.H., Yang, J.S., Robinson, P.T., Xu, X.Z., Ba, D.Z., Li, Y., Zhang, Z.M., and Rong, H., 2016a. Diamonds and Other Exotic Minerals Recovered from Peridotites of the Dangqiong Ophiolite, Western Yarlung-Zangbo Suture Zone, Tibet. *Acta Geologica Sinica* (English Edition), 90(2): 425–439.
Xiong, F.H., Yang, J.S., Ba, D.Z., Gao, J., Lai, S.M., and Zhang, L., 2016b. The feature and tectonic setting of chromitite from the Jiesha ophiolite in the Eastern Yarlung-Zangbo in Tibet. *Acta Geologica Sinica*, 90(11): 3099–3113 (in Chinese with English abstract).
Xu, D.M., Huang, G.C., Huang, L.Q., Lei, Y.J., and Li L.J., 2006. The origin of mantle peridotites in the Daba-Xiugugabu ophiolite belt, SW Tibet. *Geology and Mineral Resources of South China*, 3: 10–18 (in Chinese with English abstract).
Xu, D.M., Huang, GC., and Lei, Y.J., 2007. Origin of the Xiugugabu ophiolite massif, SW Tibet: evidence from petrology and geochemistry. *Geotectonica et Metallogenia*, 31: 490–501 (in Chinese with English abstract).
Xu, D.M., Huang, G.C., and Lei, Y.J., 2008. Chemistry and tectonic significance of mantle peridotites from the Laangcuo ophiolite massif, southwest Tibet. *Acta Petrologica Et Mineralogica*, 27(1): 1–13 (in Chinese with English abstract).
Xu, X.Z., Yang, J.S., Guo, G.L., and Li, J.Y., 2011a. Lithological research on the Purang mantle peridotite in western Yarlung-Zangbo suture zone in Tibet. *Acta Petrologica Sinica*, 27(11): 3179–3196 (in Chinese with English abstract).
Xu, X.Z., Yang, J.S., Ba, D.Z., Guo, G.L., Robinson, P.T., and Li, J.Y., 2011b. Petrogenesis of the Kangjinla peridotite in the Luobusa ophiolite, Southern Tibet. *Journal of Asia Earth Sciences*, 42(4): 553–568.
Yang, J.S., Xu, X.Z., Li, Y., Li, J.Y., Rong, H., Ba, D.Z., and Zhang, Z.M., 2011. Diamonds recovered from peridotite of the Purang ophiolite in the Yarlung-Zangbo suture zone of Tibet: A proposal for a new type of diamond occourrence. *Acta Petrologica Sinica,* 27(11): 3207–3222 (in Chinese with English abstract).
Zhang, Q., Qian, Q., and Wang, Y., 2000. Rock assemblages of ophiolites and magmatism beneath oceanic ridges. *Acta Petrologica Et Mineralogica*, 19(1): 1–7 (in Chinese with English abstract).

About the first and correspcnding author

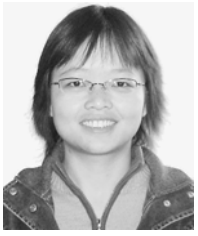

XU Xiangzhen, female, born in 1980 in Dongyang City, Zhejiang Province; doctor; graduated from Chinese Academy of Geological Sciences; associate professor of Institute of Geology, Chinese Academy of Geological Sciences. She is now interested in the study on ophiolites and mantle minerals. Email: xuxiangzhensjl@aliyun.com; phone: 13521231149, 010-68990674.